COMPARING HIGH-RESOLUTION TOPOGRAPHIC SURVEY METHODS

FOR ASSESSING GEOMORPHIC CHANGES OF POINT BARS

by

Coty Cribb

A thesis submitted to the Faculty of the University of Delaware in partial fulfillment of the requirements for the degree of Master of Science in Geology

Fall 2017

COMPARING HIGH-RESOLUTION TOPOGRAPHIC SURVEY METHODS

FOR ASSESSING GEOMORPHIC CHANGES OF POINT BARS

by

Coty Cribb

Approved: _____
Michael A. O'Neal, Ph.D.
Professor in charge of thesis on behalf of the Advisory Committee

Approved: _____
Neil Sturchio, Ph.D.
Chair of the Department of Geological Sciences

Approved: _____
Estella Atekwana, Ph.D.
Dean of the College of Earth, Ocean, and Environment

Approved: _____
Ann L. Ardis, Ph.D.
Senior Vice Provost for Graduate and Professional Education

ACKNOWLEDGMENTS

I would like to thank my parents for seeing what I was capable of when I didn't see it and always pushing me to achieve the next goal. I would not have completed this degree were it not for their support. I would like to thank my friends for their unwavering support and kindness. Finally, I would like to thank the Geology faculty at the University of Delaware for going above and beyond the thankless job of teaching to put me in a position where I can succeed for the rest of my life. I would like to specifically thank Dr. Michael O'Neal, Dr. Claire O'Neal, and Dr. John Madsen for their guidance and assistance in all matters of research and life. They have shown me how to be a successful, competent, and kind scientist directly through their own actions.

TABLE OF CONTENTS

LIST OF TABLES

LIST OF FIGURES

ABSTRACT

Detailed topographic landform analyses are the foundation of many geomorphologic investigations. Terrestrial laser scanning (TLS) is the favored survey method for studies that require high-resolution surface models; however, practical considerations, such as the high cost of instrumentation and intensive field work required to implement this approach, present possible limitations for its use in budget-limited or large-area studies. In contrast, a promising alternative approach for collecting high-resolution geospatial data collection using close-range digital photogrammetry (CRDP) provides rapid results for large study areas with a low cost-of-entry. However, the lack of published data obtained regarding CRDP methods and results makes it difficult to know if the resolution and accuracy of resultant survey data is comparable to TLS. In this study, we compare the practical issues, data collection, data processing, and results obtained from a time-series of annual TLS and CRDP surveys, performed in tandem over three years, to monitor the spatial patterns of erosion and deposition along a point bar in White Clay Creek, Newark, Delaware. Evaluation of the differences between CRDP and TLS surface models reveals that the two methods produce dissimilar digital elevation models, largely due to how each method detects bare earth and vegetation differently. As such, the volumetric change measurements of erosion and deposition along our study point bar differ significantly between the two methods. Our results suggest that in rough, obstructed, and dynamic terrains, CRDP may not be suitable high-resolution topographic survey method. However, a holistic view of survey design considerations (i.e. desired spatial resolution, the need for high resolution multispectral orthoimages, total project budget,

and field time) may require the consideration of CRDP as a heuristic survey method for many applications.

Chapter

INTRODUCTION

In recent decades, terrestrial laser scanning (TLS) and close-range digital photogrammetry (CRDP) have become commonly used by geomorphologists seeking to obtain detailed topographic models of dynamic landscapes. Both remote sensing techniques allow researchers to rapidly survey geographic areas in the range of 10^2 m2 to 10^4 m2 and obtain a dense spatial coverage of elevation data not possible with traditional survey methods (Bertin and Friedrich, 2016; Brodu and Lague, 2012; Dietrich, 2016; Fonstad et al., 2013; Hohenthal et al., 2011). The output of both TLS and CRDP is a large dataset of topographic measurements, which are typically converted into high-resolution digital elevation models (DEM) and often repeated over time to quantify geomorphic change (O'Neal and Pizzuto, 2011; Pietro et al., 2008; Prokop and Panholzer, 2009; Resop and Hession, 2010; Travelletti and Oppikofer, 2008).

Both TLS and CRDP data can be transformed into visually reasonable representations of the survey terrain. However, the methods by which the two techniques detect and/or sense the ground surface differ significantly, and may result in different spatial density and coverage of a survey area. TLS, an active remote sensing system, directly measures the distance to a surface by recording the travel time of light emitted from the scanner and reflected from surfaces. In contrast, CRDP, a passive remote sensing system, collects overlapping imagery with cameras and then relies on intensive calculations to measure the geometry of relief detected within the

1

images. Although the imagery can be collected from the ground, within predominantly flat-lying terrains CRDP imagery is often collected from the air using small unmanned aerial vehicles. In theory, if the two techniques were used to survey the same area at the same time, the topographic data collected and the resultant DEMs produced would be nearly identical. However, in practice, because of the inherent differences between the instruments and processing, significantly different DEMs of the same surface may be a likely outcome in some difficult to survey terrains. Known sources of error in both techniques arise from occluded terrain and positional uncertainty of ground control points. CRDP presents additional possible sources of error from nonlinear distortions introduced during its data processing phase (Javernick et al., 2014) and uncorrectable lens distortion from cameras (Chandler et al., 2005). The differences are without respect to subsequent statistical filtering processes applied to survey data to remove data that are suspected to not well represent the bare Earth surface. Despite the different survey, instrument, and data processing errors that can affect both data collection and subsequent DEMs, such problems are often overlooked by the end user who is focused on determining landscape changes by comparing the final elevation model from a survey. To date, few studies have undertaken the task of comparing the topographic data and subsequent DEMs produced by each method using the same study area, couched in terms of how geomorphic interpretations may be affected by the choice of instrument.

The focus of this study is to improve our understanding of how the interpretation of geomorphic changes, derived from a time-series of DEMs, would differ depending on whether TLS or CRDP is used as the survey method. We monitor topographic changes along a point bar on the White Clay Creek near Newark,

Delaware, where we collected both TLS and CRDP datasets in tandem on an annual basis over three years. We specifically (1) collected TLS data and aerial imagery on the same day once each year for three years; (2) generated TLS and CRDP digital elevation models depicting the topography and landcover distribution over the point bar; (3) used ratios of the color and near-infrared imagery to characterize landcover types over the study area; (4) assessed how intrinsic properties of different landcover types affect the data collection and subsequent elevation data; and (5) calculated DEMs of difference through time as observed with each survey method. Our results provide significant insights into each technique's practicality for accurate, efficient, and cost-effective topographic monitoring on a dynamic landscape with mixed landcover types. Our study is especially timely, as economic pressures on researchers increasingly place limits on the temporal and spatial scope of field efforts and data collection, thus inherently encouraging the use of inexpensive and widely available CRDP equipment over the more expensive and difficult-to-maintain TLS survey stations. We also seek to inform river restoration and monitoring projects like ours, which increasingly rely on high-resolution survey methods for accurate, repeated spatial assessments of geomorphic changes over time, by evaluating the practical aspects of field conditions and instrument limitations for appropriate survey design.

STUDY AREA

Our study area sits along a meander bend of White Clay Creek, Newark, Delaware which lies on the piedmont near the coastal plain transition (Figure 1). The area is mostly forested, with nearby residential neighborhoods and small farm agriculture in all directions and an urbanized area a few kilometers downstream (Figure 1). The 1664 m^2 study area was selected because of the active sediment reorganization that has been observed in previous research studies and its inclusion in ongoing funded research projects (Almendinger, 2004; Orefice, 2015; something new with Jim and me). At our study site, the White Clay Creek (WCC) is a 5th order, single channel stream with mean daily discharge of 2.7 m^3/s and flood stage of 2.9 m as measured just upstream in Stricklersville, PA (U.S. Geological Survey gauging station 01478650). At the study locale, the river flows through a mixed bedrock alluvial setting, underlain by the Wissahickon formation (Ordovician pelitic schist and gneiss), with Baltimore gneiss and Cockeysville marble outcropping upstream in southeastern Chester County, PA. The inside meander bend consists of mud to gravel deposits while the steep cut bank is mostly mud. The meander begins with a shallow riffle at the head and transitions into a pool at the bend. The bend is roughly semi-circular in plan view and is mostly treeless except for three 3 m to 5 m tall young trees growing along the elevated ridge adjacent to the active channel on the point bar (Figure 1). The floodplain is vegetated with large trees lining the river and dense underbrush throughout. A natural chute-turned-walking path has remained non-vegetated, and is lower in elevation than the floodplain ridge it bisects throughout the study.

METHODS

Data Collection

Terrestrial Laser Scanning

During each April in 2014, 2015, and 2016, both TLS and aerial imagery were collected simultaneously at the study locale during single-day surveys. We selected our surveying schedule to limit the influence of dense summer-time vegetation. The TLS instrument we used was a Trimble GX Advanced Terrestrial Laser Scanner. This instrument provides data regarding the distance to surfaces in a survey domain by measuring the time of flight of emitted pulses of green light (532 nm) with a factory-tested accuracy of approximately 1.3 mm at 100 m. The distance measurements are coupled with data regarding the azimuth and zenith of the emitted pulse to place each point in a local Cartesian coordinate system that originates at the instrument. Each data point in the survey domain consists of the three-dimensional coordinates of the first surface reflection along any vector.

To capture points across a landscape, the Trimble TLS instrument rotates on its base (around a vertical axis) at user-prescribed increments to scan near and far-field features. The default setting of this instrument collects substantially greater numbers of observations from closer features than from more distant features (i.e., tens of thousands vs. a single, or no observation). The radial pattern of data collection also influences the resolution of the final surface model that will eventually be developed from the data, because the rotational increment chosen will determine the size of the smallest features that can be detected in far-field areas.

The product of a TLS survey is a detailed, three-dimensional point cloud representative of all reflective surfaces scanned. Each data point minimally has a Cartesian coordinate within three-dimensional space (X, Y, and Z coordinate), and additionally may contain a laser return-intensity value as well as color information estimated by an on-board camera as red, green, and blue (RGB) values. The raw point cloud model typically requires filtering and other data reduction to produce a bare-earth model of the scanned surface.

The local Cartesian coordinates as well as return intensity values and true-color approximation were collected during all surveys. Measurements were taken each year from seven separate scan locations to ensure complete point-cloud coverage of the river bend. To facilitate accurate rectification between annual surveys during subsequent data processing, five permanent benchmarks were installed in early 2014, two on the upper bar and three on the cut bank side: BM1 – BM5 (Figure 1). All benchmarks were made of engraved aluminum mounted in concrete that was reinforced with steel rebar driven up to a meter into the subsurface to resist movement. In early January 2016, a large flood scoured sediment around the upstream bar-side of one of the benchmarks, prompting the installation of 3 new benchmarks in March 2016: BM6 – BM8 (Figure 1). Several temporary benchmarks (0.08 m ceramic spheres provided with the Trimble system) were centered on the permanent benchmarks (5 in 2014; 4 in 2015; 6 in 2016), with additional spheres placed throughout the survey domain (3 in 2014; 4 in 2015; 4 in 2016) to enable multiple scans from a single year to be co-registered in post-processing. The spherical shape of the temporary benchmarks limits registration errors because the mathematically modeled central point is easy to determine from different scanner locations. Each

spherical benchmark was positioned to ensure visibility from different survey stations. The product of these surveys was a set of overlapping scans acquired from each of the 7 survey stations.

<center>Close-Range Digital Photogrammetry</center>

All CRDP imagery was collected to coincide in time and space with TLS surveys using small sport cameras mounted to the bottom of a consumer-grade quadcopter. In 2014, a GoPro Hero 2 sport camera was flown over the study area, collecting 5 megapixel (MP) RGB JPEG images every 5 seconds. In 2015, two CRDP flights were undertaken; one using an SJ4000 camera collecting 10 MP RGB JPEG images, the second using a similar, 10 MP SJ4000 camera, modified to collect images in the near-infrared (NIR) spectrum (Rabatel et al., 2011). In 2016, two flights were completed using a Xiaomi YI 16 MP RGB sport camera with the lens refocused to a distance of 40 m (Liang, 2016). A third flight was completed a few days later, on April 18, 2016, at 11:00 AM (a different time-of-day than the RGB flights) using again the 10 MP SJ4000 sport camera modified to collect NIR imagery.

Please see Appendix A for a detailed overview of our data collection procedure.

<center>**Data Processing**</center>

<center>Terrestrial Laser Scanner</center>

For each dataset collected from the annually repeated surveys, the following raw point data processing procedure was followed. For each year's survey, the Cartesian coordinates of the individual ceramic spheres were used to align and register the 7 overlapping scans. The location of a single sphere within an individual scan was

<center>7</center>

matched to the same sphere location in as many other scans as possible. This was performed multiple times for many spheres within each scene to align and reduce error in three-dimensional placement. A root mean square error (RMSE) of the distance between these coordinate pairs was calculated to assess an error of fit using the centroid calculated for each sphere from each survey station. In this study, we used the highest registration RMSE value calculated for each site and refer to this error as the registration error (Table 1). To compare data between annual surveys, the point clouds were co-registered to the survey marker coordinates obtained from the 2014 survey. The end products of scan registration were three datasets, one from each survey year all using the same cartesian coordinates. We note that each year's TLS survey data generated its own Cartesian coordinate system, independent of any other survey event. Geo-referencing the point clouds with real world coordinate systems were not completed to avoid introducing a constant positional error, often add as much as a few centimeters, into all data sets (Lichit, 2005; Coveney et al, 2011).

<p style="text-align:center">Close-Range Digital Photogrammetry</p>

The image processing to develop topographic data is an intensive workflow and requires specialized software, specifically we used Photoscan Pro by Agisoft (Agisoft, 2015). Our workflow begins with selecting ten images to build a rudimentary scene based on their complete view of the bar, inclusion of GCPs, and approximate equidistant centroid spacing. Five benchmarks were identified in the images; these were added manually as control points to the images. An additional 10 stationary objects, such as large rocks, large logs, base of trees, and/or spheres not located on benchmarks, that could be identified on the bar's surface and located in all images, were also manually added as control points. The images were aligned, anchored by the

control points and up to 4,000 other key points with the greatest likelihood of matching, using full image resolution (e.g., Morgan et al., 2017). We used unlimited tie points to create a sparse cloud. These settings were used in all subsequent alignments.

The rudimentary CRDP scene was then manually projected onto the coordinate space of the concomitantly collected TLS survey by assigning the TLS-derived Cartesian coordinates to each benchmark and GCP; the rudimentary scene was then realigned. The sport cameras we used to survey have attributes that create image distortions, specifically; short focal lengths and wide-angle lenses. Agisoft recommends using their software, Lens, to correct image distortions but, due to the short focal length of our camera lenses, we could not capture a useable image of their correction grid. Instead, we improved calibration using GCP coordinates to calibrate the images in Photoscan's Camera Calibration tool per the developer's recommendations (Agisoft, 2015). Once calibrated, the projected scene was realigned a final time to reduce positional error.

To build the scene, additional images were added recursively in batches of ten. Benchmarks and stationary objects were identified in each new set of ten; using the same TLS-based Cartesian alignment protocol as before, the images were aligned, calibrated, and aligned again to minimize positional error. Lastly, a triangular mesh was generated in Photoscan Pro using the high facet setting and overlaying an image mosaic to create a final 0.1 m ortho-rectified areal image used, along with the final point cloud, for further analyses. The 2015 and 2016 NIR data were processed similarly as the aforementioned color imagery. The end products of our scene-building

workflow were the following five datasets containing a point cloud and orthoimage: 2014 RGB, and both RGB and NIR scenes for 2015 and 2016.

Please see Appendix A for a detailed overview of our data processing procedure.

Landcover Classification

Because of the differences in landcover types within our survey domain (i.e., bare earth, dry vegetation, and green vegetation) a portion of this study focused on determining how each landcover type influenced topographic measurements collected. The limited number of landcover types observed could be readily separated using color and NIR imagery. Under ideal circumstances, vegetation type and health could be discriminated using band ratios (such as: the normalized difference vegetation index (NDVI)). Five band ratios from RGB and NIR imagery were used to perform a supervised classification of 3 classes (bare earth, green vegetation, and dry vegetation) for imagery collected in 2015 and 2016 (no NIR imagery was collected in 2014).

Please see Appendix A for a detailed overview of our landcover classification procedure.

DEM Generation

The large Cartesian coordinate point data sets resulting from both TLS and CRDP processing were distilled into 0.1 m DEMs with summary statistics (point density, minimum elevation, average elevation, standard deviation of elevation, and elevation range) calculated by evaluating the data within an arbitrary 0.1 m × 0.1 m cell. The DEMs allowed for elevation (volume) change detection within the survey domain via direct cell-to-cell comparison (Sawaya et al., 2003). Interannual

comparisons were made by subtracting values of the 2014 DEM from the corresponding cell values in the 2015 DEM, and similarly, the 2015 DEM cell values from the 2016 DEM. This yielded a deviation in elevation value for each cell, representing change that occurred during the year. For each method (TLS or CRDP), a cumulative error was calculated from the sum of the errors associated with instrument error, registration, and rectification. In reference to the previous section on landcover type, each cell was assigned a single landcover type (bare earth, green vegetation, dry vegetation) via supervised classification.

To better understand differences recorded by the different survey techniques, we also analyzed several 2 m × 2 m typological sections of each landcover type. We identified three 4 m^2 areas within the study site that consistently classified as the same landcover type in each of surveys: (1) sand to gravel, (2) mud to sand, and (3) dry vegetation and grasses. These areas were selected for describing landcover type differences, specifically: (1) the sand to gravel area chosen signifies bare earth with high roughness, (2) mud to sand as a stand-in for bare earth with low roughness, and (3) ground cover and grasses that represent a partially occluded area. Then, each of the three areas was clipped from the six surface models. Interpolation of missing data was completed using three methods common to geomorphologists: 1) natural neighbors, 2) inverse distance weighting, and 3) kriging. Through a detailed analysis of the differences in the output surface models of TLS vs CRDP in each of these three areas, we test the influence of roughness, high relative relief, and occlusion on surface model production in both methods. Within each of the three typographic areas, elevation-difference datasets were also created by subtracting the minimum elevation value of

each cell of 2014 from 2015, and 2015 from 2016 for both survey methods and all three interpolation methods.

RESULTS

The TLS surveys yielded 1554330 total data points in 2014, 7334024 total data points in 2015, and 5561876 total data points in 2016 (Table 1). Many of these data are of from far field return outside of our specific study area. Thus, within the bounds of our 1664 m2 study area, 1258841 data points were measured in 2014, 6878297 in 2015, and 1923149 in 2016 (Table 1). TLS positional errors fluctuate a few 0.01 m's but are generally stable year to year (Table 1). In our TLS surveys, we recorded point density per cell averages of 8 points in 2014, 41 points in 2015, and 12 points in 2016 (Figure 2 and Table 1). We produced a DEM for each survey using the minimum elevation for each 0.1 m cell (Figure 3). We summed the cells with deposition separately from the cells with erosion. Between 2014 and 2015, TLS surface models show 63.09 m^3 of erosion, 30.09 m^3 of deposition, and total absolute volumetric change of 93.18 m^3 (Figure 4). The 2015-2016 TLS difference models show 36.02 m^3 of erosion, 49.00 m^3 of deposition, and total absolute volumetric change of 85.02 m^3 (Figure 4).

The CRDP surveys collected 46 images in 2014, 40 images in 2015, and 39 images in 2016. Photogrammetric analyses of these images resulted in 2250050, 2017800, and 1526503 topographic points in 2014, 2015, 2016, respectively. However, a much smaller fraction of these points fell within our study area as compared to that of the TLS surveys; 381847 in 2014, 378379 in 2015, and 304242 in 2016 (Figure 2 and Table 1). The low number of data points collected resulted in a mean point density of 2 points per 0.1 m cell for all three years, with a maximum of 13

points observed in any 0.1 m cell. This stands in stark contrast to the higher mean point densities observed in TLS surveys (Table 1). CRDP surface models from 2014-2015 suggests 154 m^3 of erosion and 44 m^3 deposition with a total absolute volumetric difference of 199 m^3 (Figure 4), more than double that recorded by the TLS survey. Again, the 2015-2016 CRDP difference models document larger volumes of change in all categories when compared to the TLS difference models, documenting over three times as much erosion (138 m^3), ~1.5 times greater deposition (70 m^3), and a total absolute volumetric change of 209 m^3 (Figure 4), more than double that recorded by the TLS survey.

We note, however, that both TLS and CRDP created regions of data-blindness (Figure 2). In our TLS surveys, the radial nature of the TLS data collection at each station, the presence of dense vegetation, and/or relatively steep localized relief created regions with areas 946 m^2 (2014), 730 m^2 (2015), and 611 m^2 (2016) that were occluded from multiple scan locations. We also observed that CRDP methods result in areas of data-blindness – 62 m^2 (2014), 53 m^2 (2015), and 141 m^2 (2016) throughout our study area – but unlike with TLS, these areas do not result from simple low-angle occlusions, but rather a statistical inability to identify terrain elements in the imagery.

Next, we compared the elevation differences between TLS and CRDP surface models in the same year as a difference over the entire 1664 m^2 study area, to better understand in the broader sense dissimilarities between the surface models. The absolute value of all elevation differences, summed, between TLS and CRDP surface models were recorded as: 46 m^3 net difference in 2014, 68 m^3 net difference in 2015, and 104 m^3 net difference in 2016. Of course, this average incorporates both deposition (positive cell values in DEMs-of-difference) and erosion (negative cell

values in DEMs-of-difference) and therefore does not fully represent change in either direction.

Landcover classification of data from 2015 parsed the study site's subaerial landcover into the following categories: >1% green vegetation (8 m^2), 16% dry vegetation (248 m^2), and 42% bare earth (692 m^2). Similarly collected data from 2016 showed increased green vegetation, totaling 8% (135 m^2), increased dry vegetation at 31% (514 m^2), and less bare earth terrain at 29% (466 m^2) (Figure 5). Thus, between 2015 and 2016, areas of bare earth decreased, while vegetation increased.

Summary statistics were compared between the different landcover types of TLS and CRDP surface models by calculating the root mean squared error (RMSE). This comparison showed a steady increase in the elevation difference measurements over the entire study through time. From 2014 to 2016: the minimum elevation difference increased from 0.09 m to 0.18 m, the mean elevation difference increased from 0.10 m to 0.20 m, and the elevation range difference increased from 0.12 m to 0.30 m (Table 2). Bare earth and dry vegetation follow the increasing difference trend but green vegetation does not, being more different during the 2015 survey than 2016.

To view the topographic differences between landcover types from different perspectives hypsometric curves (Figure 6) a cross section of the raw points and DEM (Figure 7) were completed. These visual aids help to see differences between how the methods record landcover type at large and small scales.

Additionally, we undertook a visual comparison of the 18 possible combinations of both DEM generating methods (TLS and CRDP), three different landscape types, and three different summary statistics (details in APPENDIX B, Figures 8 – 25).

The three typographic areas presented in APPENDIX B illustrate important similarities and differences between how both methods record topography. For typographic area 1 (sand to gravel), both TLS and CRDP methods are consistent in the way they measure the average, minimum, and maximum elevation (Figures 8, 9, and 10), e.g. the elevation value does not change regardless of which statistic is used. When comparing method to method, the minimum elevation shows a northwestern dipping slope recorded by both methods but the shape is offset vertically by a few decimeters between methods. Additionally, between methods, there is a drastic point density difference (Figure 11) and very similar range and standard deviation (Figures 12 and 13). Typographic area 2 (mud to sand) shows the same relationship between elevation statistics, point density, range and standard deviation (Figures 14, 15, 16, 17, 18, 19) as typographic area 1. Typographic area 3 shows similar relationships between the elevation statistics and point density as typographic area 1 (Figures 20, 21, 22, 23) but very different range and standard deviation measurements between methods (Figures 24 and 25) with TLS recording a 3D "cloud" of points while CRDP records a 2D "surface" of points.

For typographic area 1 (sand to gravel), both TLS and CRDP agree that erosion occurred between 2014-2015 and deposition occurred between 2015-2016; however, in both cases, CRDP measures a greater total volume of erosion and deposition – 42% greater in 2014-2015 and 49% greater in 2015-2016, compared to TLS (Table 3). We found that for every other typographic area and annual interval, TLS and CRDP interannual difference maps did not agree in amount or direction of volumetric change (Table 2). For example, in typographic area 2 (mud to sand), TLS difference maps displayed a deposition of 0.28 m^2 between 2014-2015, while CRDP

recorded an erosion of 0.34 m^2; between 2015-2016 the survey techniques recorded the opposite, with TLS maps showing 0.09 m^2 of erosion and CRDP-derived maps showing 0.67 m^2 of deposition (Table 3). Any contribution to these reported volumetric differences by interpolation method appears to be negligible; in all cases, the calculated volumetric differences agreed well among the three interpolation methods used, showing that differences between our chosen clipped areas occur irrespective of whether kriging, nearest-neighbors, or inverse distance weighting was used. In general, our results show that typographic area 1 (coarse bare earth) presents a best, but not ideal, case for agreement between survey methods and that landcover type affects our ability to detect volumetric changes in a dynamic fluvial landscape.

DISCUSSION

Over a three-year period (2014-2016), TLS and CRDP surveys captured point bar accretion at our study site along White Clay Creek. Between each year, both survey methods produced overall difference maps that were in agreement with respect to the general nature of sediment redistribution along the channel. However, as we have demonstrated, the measured volumes differ greatly between the methods, with CRDP consistently detecting greater amounts of sediment redistribution than TLS. Influencing and potentially causing this disagreement are differences on the order of a few cells in any direction, as demonstrated by our study of typographic landcover sites. Differences of volumetric measurements over vegetated land cover types were especially large, yielding DEMs-of-Difference that differ between survey methods by up to two orders of magnitude at 0.1 m raster resolution.

Our observed differences between volumetric measurements can be explained by comparing the means and scale of data acquisition. Intrinsic to both methods' topographic measurements are differences in the way data is collected, which will inevitably produce significant qualitative error. First, TLS and CRDP methods inherently differ in their ground sample distance (GSD); the smallest feature able to be resolved by the method. In practice, a feature must be many times larger than the GSD to identify or model the feature above error. CRDP smooths high frequency undulations in topography that are smaller than a few times the GSD, with the effect of simplifying topography. In contrast, TLS under-samples most topography because the GSD detected by TLS is orders of magnitude smaller than the form it is measuring. However, TLS compensates for under sampling with its data richness, often collecting 10^2 to 10^3 measurements within a 0.1 m $\times$ 0.1 m area, while CRDP data density cannot exceed the GSD of the initial images, thereby limiting maximum resolution.

In non-bare earth areas, the GSD difference is exaggerated by the perspective with which each technique views the landscape. Recall, TLS scans terrain as a side-on view and CRDP scans terrain from a birds-eye view. Just as dense brush obscures the surface of the land from the human eye, neither TLS nor CRDP is capable of accurately measuring ground surface through densely packed green and dry vegetation. At best, TLS's lateral perspective and small GSD may result in point-returns able to travel through chance, tiny gaps in dense vegetation; more typically, the presence of dense vegetation results in lateral occlusion, requiring the surveyor to station the instrument at multiple scan locations to ensure complete coverage throughout the desired scene (Coveney and Stewart Fotheringham, 2011). In contrast, CRDP's aerial perspective and coarser GSD produces a nearly complete, laterally

continuous model of the landscape. However, areas of dense vegetation create vertical occlusion that, in the absence of other data, may misrepresent the vegetation canopy as ground elevation. Additional physical limitations (i.e. high frequency surface roughness, coarse GSD, aerial sampling perspective) prohibit accurate elevation measurements in many areas. Areas of high relative relief or roughness may distort ground elevation perceived by CRDP by rounding peaks and shallowing valleys.

In comparing the spatial data produced by TLS vs CRDP, we noticed that differences in elevation between the two methods appeared exaggerated by certain landcover types. DEMs and hypsometric curves of the minimum elevation throughout the study site and within each landcover type (Figure 6, 10, 16, 21), shows that TLS and CRDP record the same general shape of topography but that the finer topographic details are offset, smoothed, or stretched when compared to each other. This interpretation is reinforced by Table 3 and an illustrated relationship between the raw point clouds, surface models, and landcover types in a 0.1 m wide swath cross section of the 2016 surveys (Figure 6), which suggests that the TLS laser-return records a greater range in elevation in vegetated areas by capturing the full vegetation depth, while CRDP, with smaller elevation ranges and smaller standard deviation, only captures the vegetation canopy.

We thus expected mostly identical bare earth representations between survey methods, as bare earth areas present fewer obstructions to occlude or distort TLS's laser or CRDP's line of sight. However, our results indicate TLS and CRDP do not record bare earth topography similarly. Our analysis of two typological bare-earth sub-sections of the larger study site found that both methods agree with respect to the direction of sediment flux (erosion vs deposition), but disagreed with respect to the

18

magnitude of change. Disregarding obstructions, the quality of CRDP and TLS surface models depend on the distance from the target, sensor quality, lens/laser quality, and GCP quality (spatial accuracy and quantity). For TLS, these variables are factory reported with known margins of error whereas, for CRDP, these variables are difficult to accurately quantify. In the CRDP surface model, this uncertainty lends itself to many more degrees of freedom within which spatial errors and distortions may propagate. As such, we propose that the CRDP surface model is causing most of the disagreement between methods.

The differences between surface models is caused by three factors: non-linear CRDP processing distortions, uncorrectable lens distortions, and the method of converting point cloud to DEM. Take for instance, a typical shoe print in the sand. Disregarding lateral and vertical occlusion, TLS will record the imprinted shape of the shoe, the tread pattern, and the displaced sediment encircling the shoe print with 10^1 to 10^2 points per 0.1 m cell. Conversely, CRDP will only place a few points along the elevated ridge surrounding the shoe print, failing to model the tread pattern or depressed area altogether.

Similarly, consider a series of equally spaced ripples with similar amplitude in a sandy area. TLS will record the valleys, flanks, and ridgeline of each ripple with many points while CRDP will only place points on the ridgeline. Using the minimum elevation statistic both methods will bias the most representative ground surface: with TLS recording the elevation of the valley in its DEM and CRDP recording the elevation of the ridgeline for its DEM. Although for our study, the minimum elevation statistic allowed a simple and standardized means to see ground elevations through vegetated areas and was thereby justified despite its obvious downfalls. Other TLS

analyses might use a different technique that is more representative of the actual average elevation within a cell but because CRDP is data poor, those techniques would not be useful, and would obstruct our attempt to compare the surface models in their "natural" state.

Finally, picture a typical dynamic bar surface with generally sinusoidal-like features at different scales, superimposed on themselves (i.e., a mostly bare earth, downward sloping bar surface, with ripples and hummocks, superimposed on heterogeneous gravelly muddy sand). At 0.1 m resolution, the surface models will be just as dissimilar as previously discussed. However, if 0.2 m resolution surface models were used, with the same raw topographic data, the area encompassed within the cell increases by four, thereby increasing the likelihood that CRDP will measure a point within the cell boundaries that disregards roughness and debris elements at the surface and is accurately representative of the ground surface, thereby making the TLS and CRDP surface models more similar. Over bare earth areas, as the cell size increases the surface models will continue to become more similar until, at some ideal resolution, the models are identical. The ideal resolution would need to be quantified before a monitoring survey began and will vary with lens quality, sensor quality, as well as with landcover type, and roughness elements within a landcover type. Remember though, that this relationship is only valid for bare earth areas and is reversed in densely vegetated areas. For instance, in an area with dense groundcover, as cell size increases TLS will capture more points that travel through vegetation and reflect off the ground while, regardless of resolution, CRDP has no means to measure topography through dense vegetation and will model the vegetation canopy.

Measuring topography is inherently inaccurate, at some scale, no matter the survey technique that is used. With that in mind, an active remote sensing system (TLS) provides an added level of confidence because it directly measures topography that passive remote sensing techniques, such as CRDP, are not afforded due to their characteristically indirect measurement procedure. Additionally, Photoscan, used in CRDP image processing, may provide the user with a false sense of low spatial uncertainty because its self-reported positional error does not include the magnitude of difference that we observe. For instance, the self-reported positional error for all of our CRDP surface models were less than 0.06 m (Table 1) but when we compared our CRDP surface model to the spatially accurate TLS surface model of the same year we reported spatial offsets well over 0.06 m (Figure 4) suggesting that Photoscan's reported positional error does not account for all positional uncertainty.

For our type of fluvial geomorphologic analysis, CRDP is appropriate for qualitative imaging, but not quantitative measurements. A TLS based monitoring survey will better capture accurate erosion and deposition measurements (at any scale greater than or equal to 0.1 m) across all landcover types but TLS is field intensive, disrupts the natural landscape, and is expensive. Conversely, a CRDP based volumetric monitoring survey would not be applicable in a large scale, vegetated landscape at any resolution and could not achieve high resolution and high positional certainty in a bare earth landscape without such a multitude of precisely geolocated GCPs that the method would be rendered essentially impractical. While ill-suited for precise volumetric analyses in dynamic landscapes, CRDP has important practical advantages over TLS. We have demonstrated that low-cost sport cameras and do-it-yourself NIR cameras can create high resolution orthophotos useful for remote sensing

21

analysis (Rabatel et al., 2011) and mapping purposes. We agree with Hauet et al (2009) that CRDP is a convenient tool for monitoring horizontal accretion/erosion rates. For example, from CRDP-collected data, the bar edge, cut bank, or large woody debris could be digitized in plan-view and tracked through time at a very high temporal frequency (i.e., daily or weekly if needed) (Hauet et al, 2009). With more frequent aerial surveys strategically timed around the emplacement of the tree that fell during a January 2016 flood event, subsequent downstream deposition and thus horizontal accretion rates could have been visualized in great detail. We thus suggest that the initial images and orthophotos captured by CRDP would be useful in tandem with TLS surface models to document qualitative *in situ* site layouts and landcover-type spatial distributions, akin to how sidescan sonar can supplement bathymetric data for analyses in marine environments.

CRDP could be specifically useful during TLS survey design to determine the optimal locations for TLS survey stations. A low-resolution surface model could be created in the field on a standard laptop in less than an hour. This model could be input into a predesigned viewshed analysis (on the same computer) that locates optimal scanner locations, thereby reducing total occluded areas (from vegetation, topography and other obstructions), using the fewest number of survey stations, maximizing the total spatial coverage area, reducing total field time investment, and ultimately increasing surveyor confidence that a usable model has been collected. Additionally, it would provide a useful high resolution ortho-rectified base map for figures and reports.

The inherent characteristics of TLS and CRDP as candidate methods for conducting a survey in a dynamic fluvial setting are distinctly different and worth

considering carefully as part of any project's experimental design. As cost is always a factor to the practical researcher, it is worth noting that TLS instruments are about two orders of magnitude more expensive to purchase and maintain (than CRDP instruments), and typically require manufacturer's software to register a scene and interpret dense point-cloud data. A CRDP survey, on the other hand, is easily performed using an off-the-shelf quadcopter or "drone", a small camera, and free open source software. The convenience and cost that CRDP provides, however, comes at a potential trade-off in data quality, as the low data density produced by CRDP must necessarily yield a resulting DEM with greater positional error and uncertainty. If image resolution were doubled, the number of pixels per images would have a fourfold increase which would in turn increase data density but also substantially increase the computer time required to process the imagery. For now, increasing image resolution is the most efficient approach to make the CRDP surface models comparable to TLS's, but requires more sophisticated technology than simple off the shelf AUV's with small sport cameras. Alternatively, we have demonstrated that, at 0.10 m resolution, CRDP surface models in non-vegetated areas have vertical uncertainties about twice as large as their horizontal uncertainties. But, we recognize that for some analyses this level of fine detail is not required or necessary. By using the same data to make a surface model a few times coarser than 0.10 m, the ground elevation could be represented with vertical and horizontal uncertainty well within the cell size with minimal monetary investment.

FIGURES
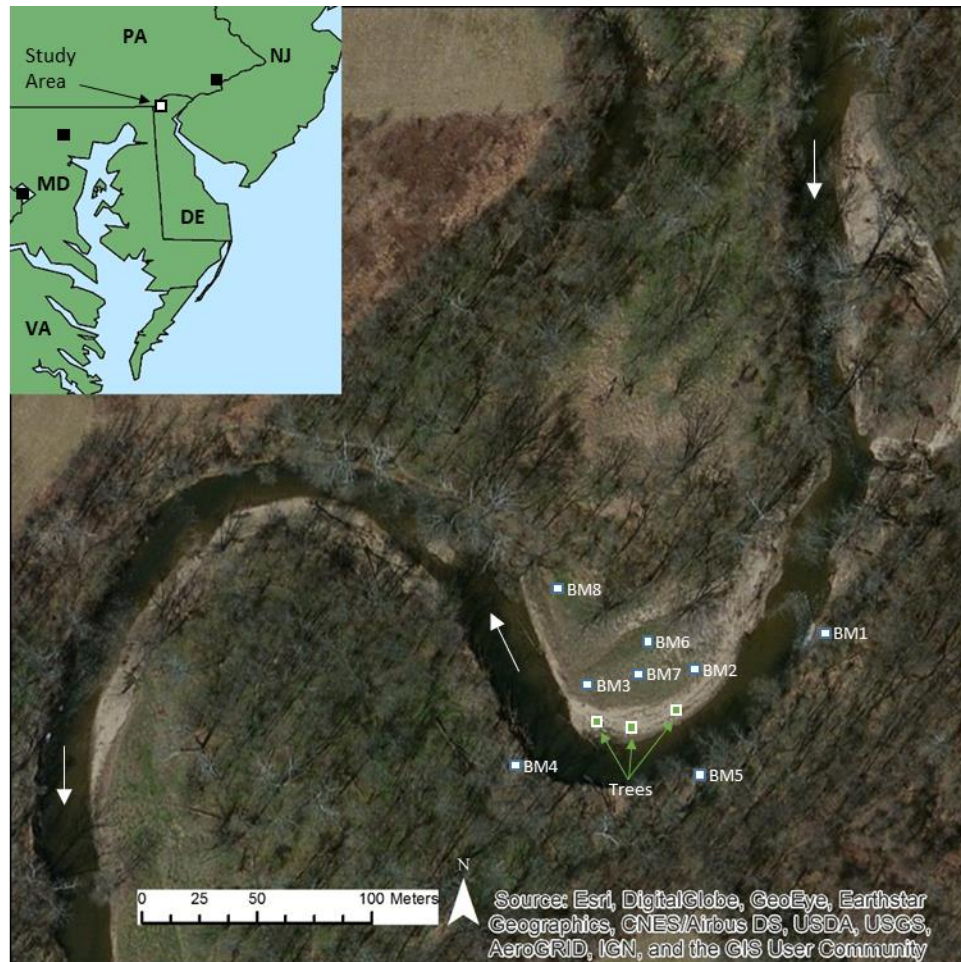
Figure 1   Study area in relation to mid-Atlantic, USA. Benchmark location also
            identified. BM1-BM5 installed before 2014 survey. BM6-BM8 installed
            before 2016 survey. There are three 3 m to 5 m trees inside study area
            bounds.
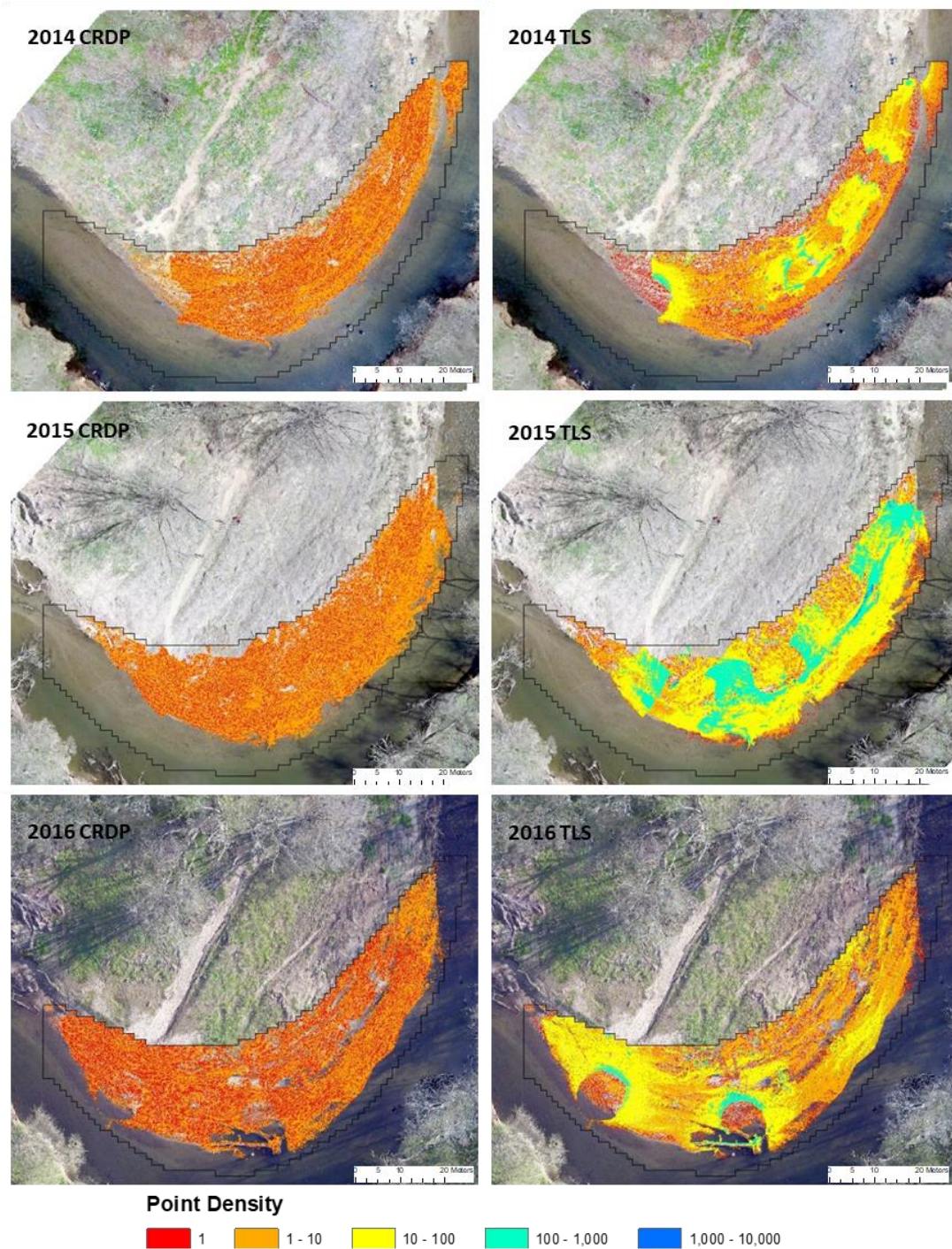
Figure 2   Comparing point density between TLS and CRDP surface models. Only areas where both methods sample the same cell are included. Notice logarithmic scale and order of magnitude point density difference between survey methods.
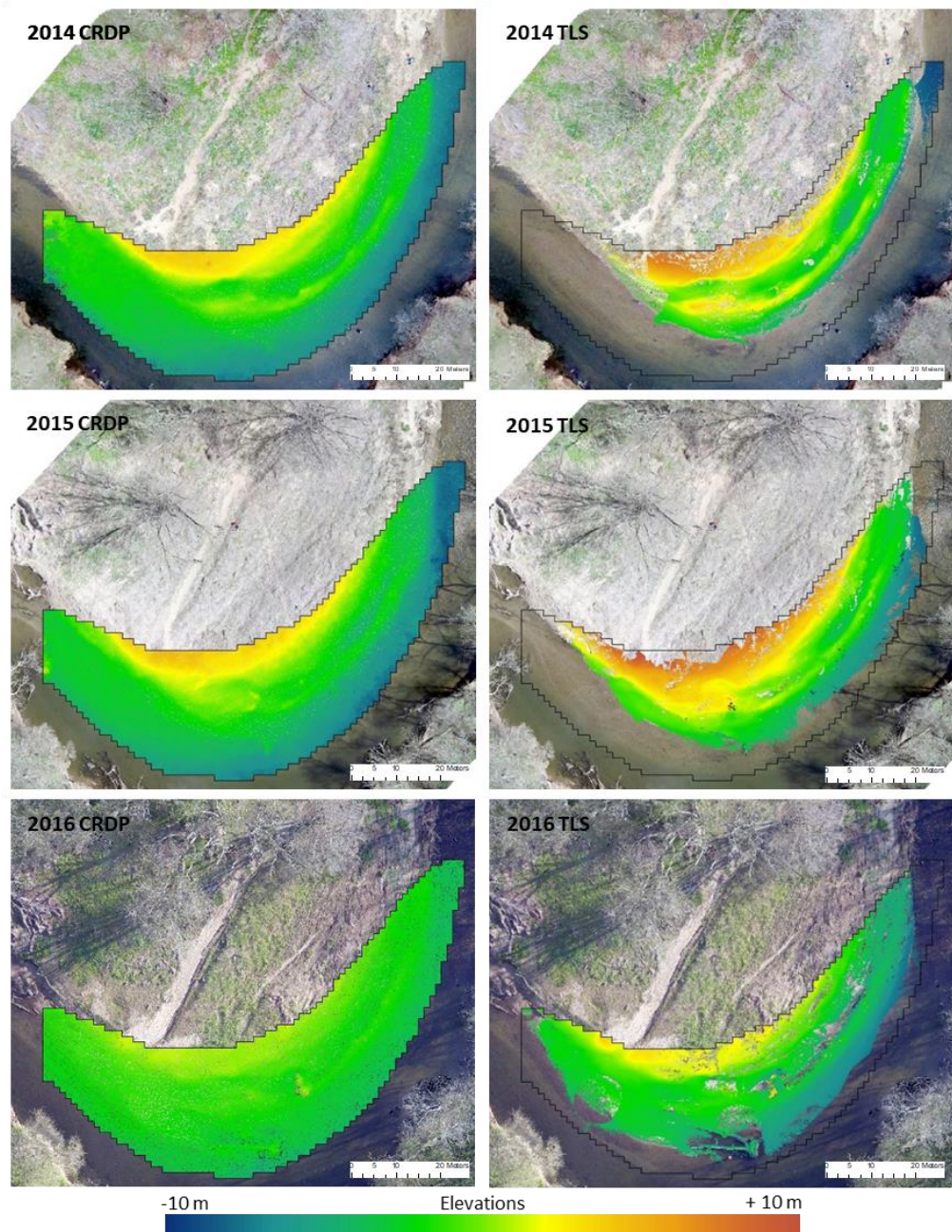
Figure 3   Digital elevation models of a point bar in White Clay Creek State Park, DE collected on April 11, 2014, April 16, 2015, and April 16, 2016 simultaneously using terrestrial laser scanning and close-range digital photogrammetry survey methods. Background orthoimages created by CRDP procedure. Notice differences in spatial coverage between methods (systematic or user created) of the same year and vegetation difference in background photos between years.

27
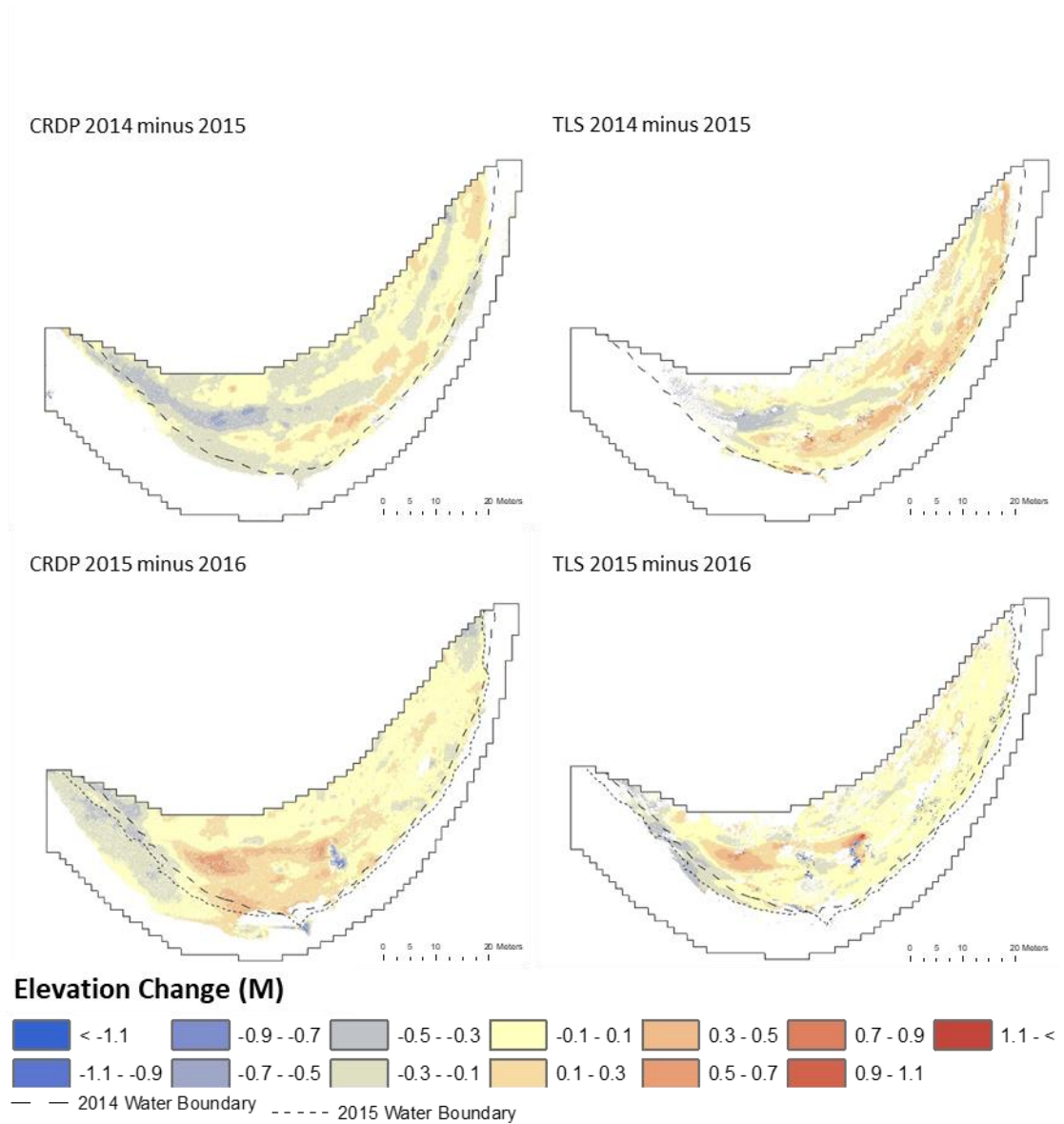
Figure 4   Annual DEM's of difference from TLS and CRDP surface models. Red
indicates areas of erosion and blue indicates areas of deposition. Notice
similarities and differences in the shape and distribution of sediment
fluxes between survey methods of the sequence.

28
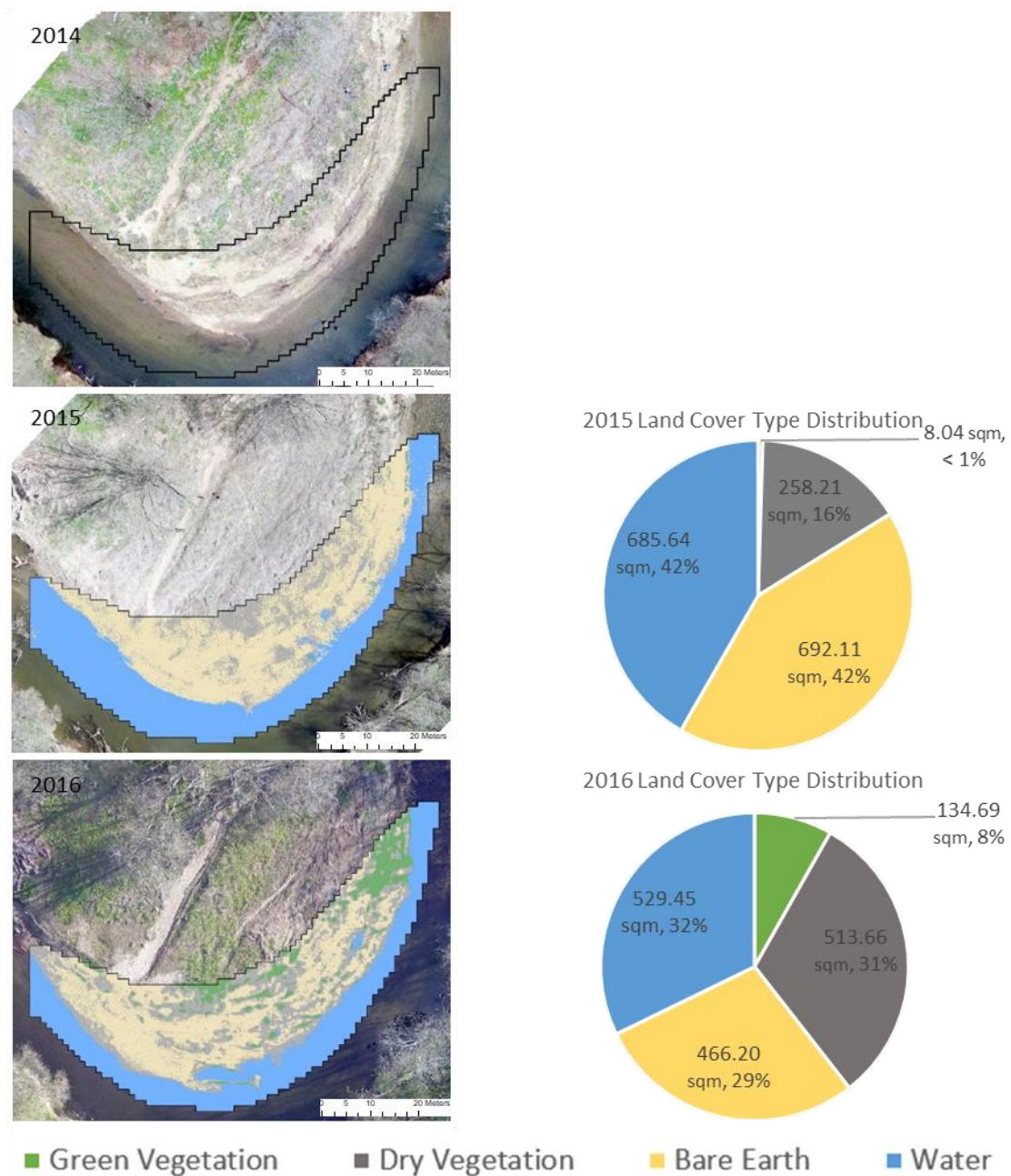
Figure 5 Left column: CRDP ortho images depict land cover type classification using multispectral band ratios as inputs for supervised classification. Right column: Pie charts display how areal coverage of landcover types changes annually over 1664 m^2 study area.

2014 10cm Elevation Comparison Histogram

2015 10cm Elevation Comparison Histogram

2016 10cm Elevation Comparison Histogram

Legend:
— • CRDP Whole — • CRDP Green Veg — • CRDP Dry Veg — • CRDP Bare Earth — • CRDP Water/Black Body
•••••• TLS Whole •••••• TLS Green Veg •••••• TLS Dry Veg •••••• TLS Bare Earth •••••• TLS Water/Black Body
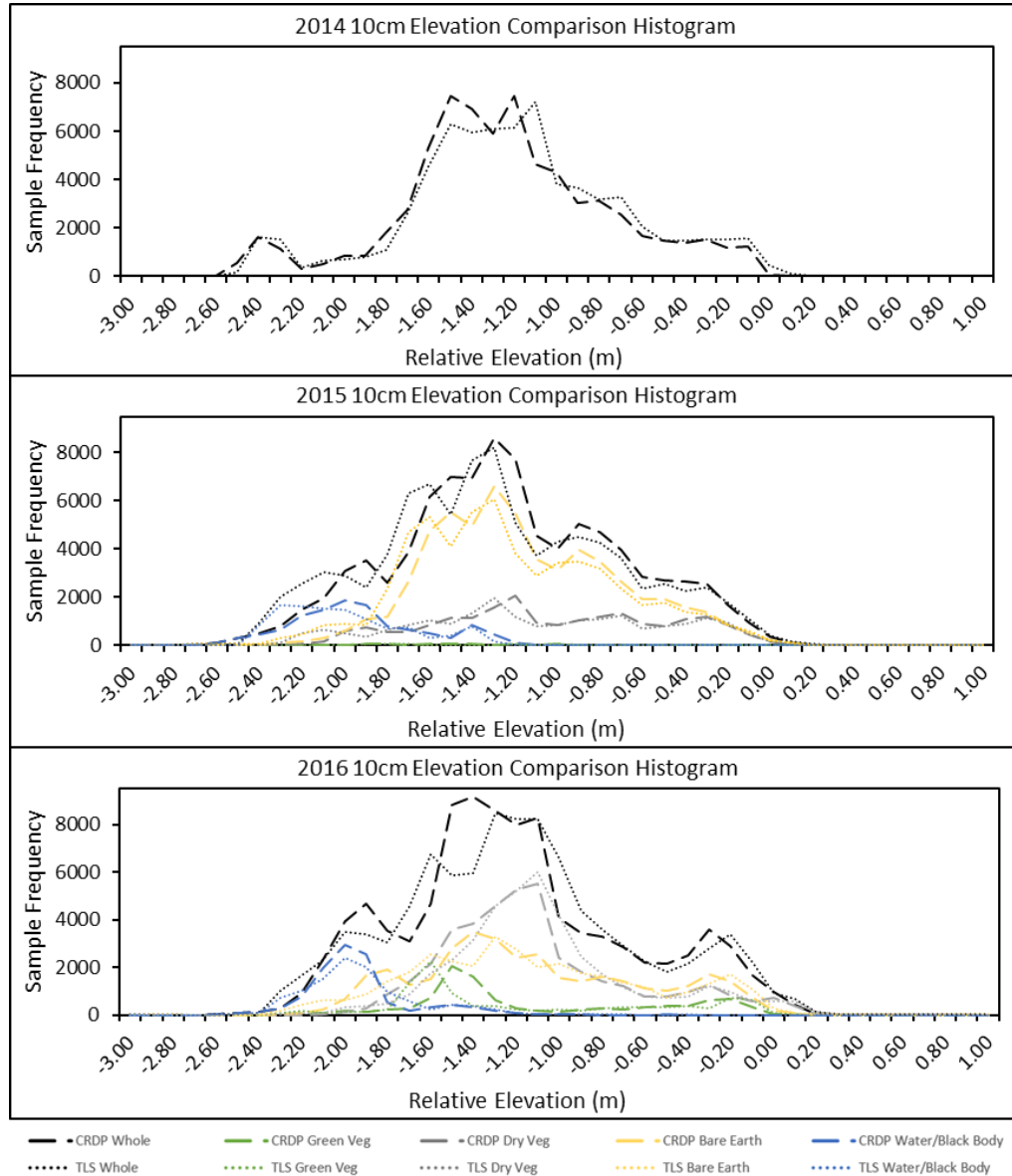
Figure 6   Hypsometric curves that are classified by land cover type for both CRDP and TLS. Only the cells that both methods measure are included for comparison. Differences between lines of the same color represent how the methods disagree while representing the same land cover type over the same spatial domain. Bin size is the same as DEM cell size: 0.1 m. Take note of the vertical offsets (viewed as horizontal shifts on the graphs) between the peaks of each method's hypsometric curves. Offsets are 1 to 3 times the cell size of 0.1 m which indicates topographic measurement disparities between methods that are larger than reported positional uncertainties.
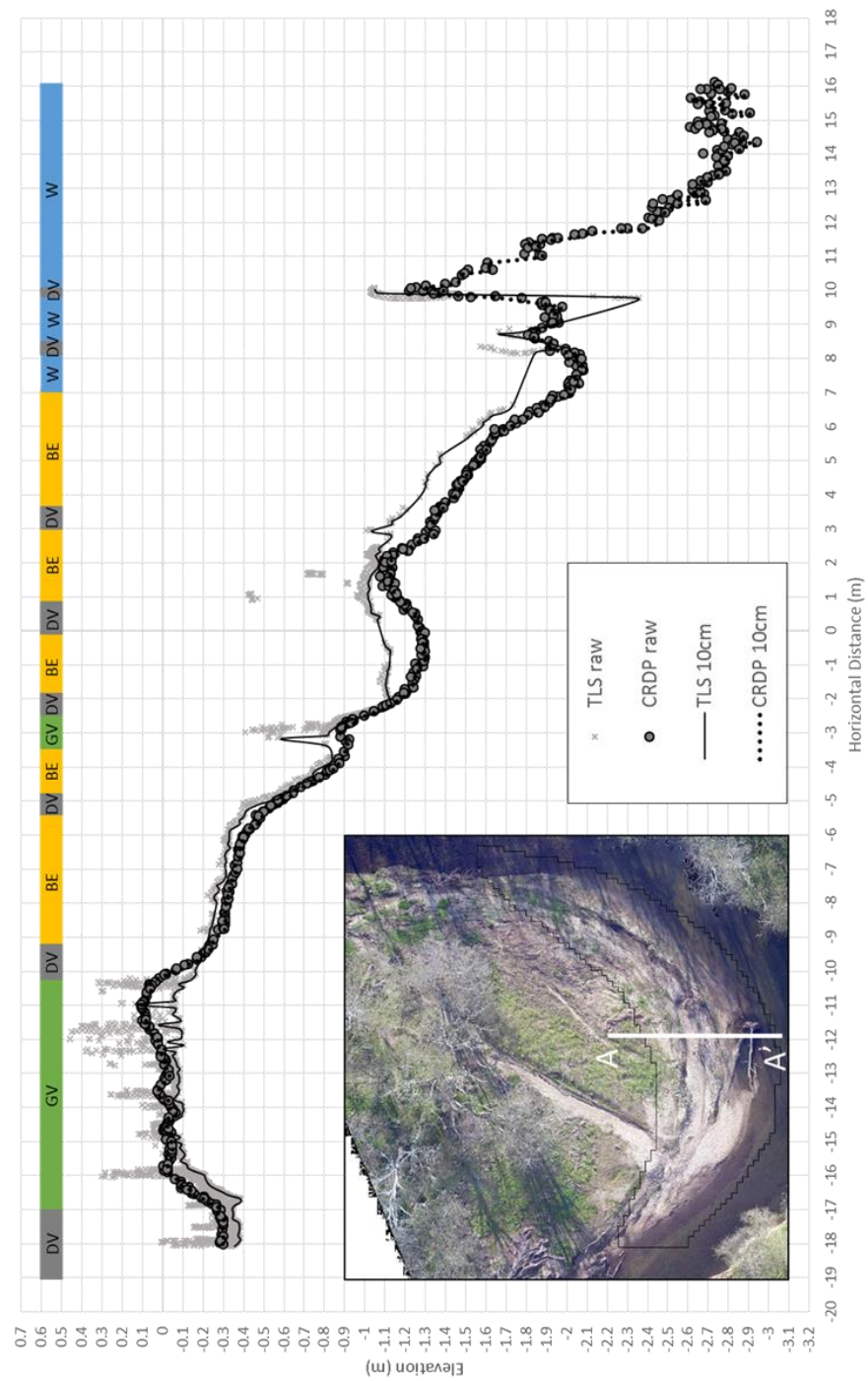
Figure 7   Cross section of raw points and the DEM surface model to compare how each method represents the surface elevation. Landcover types are noted as a colored bar across the top: DV (dry vegetation), GV (green vegetation), BE (bare earth), W (water).

TABLES

Table 1   Extent and point density comparative analysis and quantitative error analysis for both survey methods.

Survey Year	Survey Instrument	Num. of raw points	Num. of points in study area	Full spatial extent with data (m2)	Mean point density (10cm cell)	Num. of survey stations	Num. of images	Alignment RMSE (cm)	Rectification error (cm)	Total quantitative error (cm)
2014	TLS	1,554,330	1,258,841	2,744	8	7	-	1.1	0.0	1.1
	CRDP	2,250,050	381,847	15,093	2	-	46	3.2	0.9	4.1
2015	TLS	7,334,024	6,878,297	1,848	41	6	-	1.2	0.9	2.1
	CRDP	2,017,800	378,379	11,388	2	-	40	4.0	1.0	5.0
2016	TLS	5,561,876	1,923,149	8,610	12	7	-	1.0	0.8	1.8
	CRDP	1,526,503	304,242	12,031	2	-	39	5.5	1.1	6.6

Table 2   Root mean squared error (RMSE) between summary statistics of TLS and CRDP surface models separated by landcover types. Notice general trend towards higher differences in every category (except point density and green vegetation) though time.

Landcover Classification	Minimum Elevation RMSE (M)			Average Elevation RMSE (M)			Point Density RMSE (# of points)			Standard Deviation RMSE			Elevation Range RMSE (M)		
	2014	2015	2016	2014	2015	2016	2014	2015	2016	2014	2015	2016	2014	2015	2016
Whole Area	0.09	0.13	0.18	0.10	0.10	0.20	88	152	65	0.03	0.05	0.10	0.12	0.21	0.30
Bare Earth	-	0.12	0.17	-	0.08	0.20	-	159	60	-	0.05	0.10	-	0.20	0.31
Green Vegetation	-	0.24	0.16	-	0.16	0.18	-	185	28	-	0.09	0.07	-	0.37	0.22
Dry Vegetation	-	0.16	0.19	-	0.10	0.22	-	157	79	-	0.05	0.12	-	0.19	0.35

Table 3   Illustrating how landcover type influences volumetric flux measurements
            by using three different interpolation methods on small study areas. A
            negative value denotes erosion; a positive value corresponds to
            deposition. All volume change measurements are in cubic meters.

TYPOGRAPHIC AREA 1 (SAND TO GRAVEL)

Survey Method	Kriging		NN		IDW	
	2014 - 2015	2015 - 2016	2014 - 2015	2015 - 2016	2014 - 2015	2015 - 2016
TLS	-0.61	0.56	-0.61	0.55	-0.61	0.56
CRDP	-1.05	1.1	-1.05	1.09	-1.05	1.1
% Difference	42%	49%	42%	49%	42%	49%
RMSE	0.44	0.54	0.44	0.54	0.44	0.54

TYPOGRAPHIC AREA 2 (MUD TO SAND)

Survey Method	Kriging		NN		IDW	
	2014 - 2015	2015 - 2016	2014 - 2015	2015 - 2016	2014 - 2015	2015 - 2016
TLS	0.28	-0.09	0.28	-0.09	0.28	-0.09
CRDP	-0.34	0.67	-0.37	0.69	-0.34	0.67
% Difference	19%	87%	24%	88%	18%	87%
RMSE	0.62	0.76	0.64	0.78	0.63	0.76

TYPOGRAPHIC AREA 3 (GRASSES AND GROUNDCOVER)

Survey Method	Kriging		NN		IDW	
	2014 - 2015	2015 - 2016	2014 - 2015	2015 - 2016	2014 - 2015	2015 - 2016
TLS	0.49	-0.10	0.49	-0.10	0.49	-0.10
CRDP	-0.04	0.18	-0.08	0.22	-0.04	0.18
% Difference	92%	77%	84%	126%	91%	86%
RMSE	0.59	-	0.57	0.31	0.53	0.27

REFERENCES

Agisoft, (2015). Agisoft PhotoScan User Manual: Professional Edition. Version 1.0.0. Retrieved September 30, 2015 from http://www.agisoft.ru/products/photoscan/professional/.

Allmendinger, N. (2004). The influence of convex-bank floodplains on stream channel morphology in the mid-atlantic piedmont. Ph.D. Dissertation, University of Delaware, Newark.

Coveney, S., and Stewart Fotheringham, A. (2011). Terrestrial laser scan error in the presence of dense ground vegetation. The Photogrammetric Record, 26(135), 307-324.

Bertin, S. and Friedrich, H. (2016). Field application of close-range digital photogrammetry (CRDP) for grain-scale fluvial morphology studies. Earth Surface Processes and Landforms, 41(10), 1358-1369.

Brodu, N. and Lague, D. (2012). 3D terrestrial lidar data classification of complex natural scenes using a multi-scale dimensionality criterion: Applications in geomorphology. ISPRS Journal of Photogrammetry and Remote Sensing, 68(1), 121–134.

Burrows, N. (2015). *A comparative analysis of terrestrial laser scanning (TLS) and structure from motion (SfM) photogrammetry for measuring fluvial sediments.* MSc thesis, University of Salford. Manchester.

Chandler, J., Fryer, J., and Jack, A. (2005). Metric capabilities of low cost digital cameras for close range surface measurement. The Photogrammetric Record, 20(109) 12-26.

Dietrich, J. T. (2016). Riverscape mapping with helicopter-based Structure-from-Motion photogrammetry. Geomorphology, 252, 144–157.

Fonstad, M. A., Dietrich, J. T., Courville, B. C., Jensen, J. L., and Carbonneau, P. E. (2013). Topographic structure from motion: A new development in photogrammetric measurement. Earth Surface Processes and Landforms, 38(4), 421–430.

Hauet, A., Muste, M., and H-C., Ho. (2009). Digital mapping of riverine waterway hydrodynamic and geomorphic features. Earth Surface Processes and Landforms, 34(2), 242–252.

Hohenthal, J., Alho, P., Hyyppä, J., and Hyyppä, H. (2011). Laser scanning applications in fluvial studies. Progress in Physical Geography, 35(6), 782-809.

Hortobágyi, B., Corenblit, D., Vautier, F., Steiger, J., Roussel, E., Burkart, A., and Peiry,

J.-L. (2016). A multi-scale approach of fluvial biogeomorphic dynamics using photogrammetry. Journal of Environmental Management.

Javernick, L., Brasington, J., and Caruso, B. (2014). Modeling the topography of shallow braided rivers using Structure-from-Motion photogrammetry. Geomorphology, 213, 166–182.

Lichti, D. D. (2004). A resolution measure for terrestrial laser scanners. The International Archives of the Photogrammetry, Remote Sensing and Spatial Information Sciences, *34*(Part XXX), 6.

Liang, O. (2016). "Fix Xiaomi Yi Camera Lens Focus Issue." oscarliang.com/fix-xiaomi-yi-camera-lens-focus-issue/.

Morgan, J. A., Brogan, D. J., and Nelson, P. A. (2017). Application of Structure-from-Motion photogrammetry in laboratory flumes. Geomorphology, 276, 125–143.

O'Neal, M. A., and Pizzuto, J. E. (2011). The rates and spatial patterns of annual riverbank erosion revealed through terrestrial laser-scanner surveys of the South River, Virginia. Earth Surface Processes and Landforms, 36(5), 659-701.

Orefice, M. (2015). *Quantifying geomorphic change to a point bar in response to a high flow event using terrestrial lidar, White Clay Creek, Delaware*. Masters Thesis, University of Delaware, Newark.

Pietro, L. S., O'Neal, M. A., and Puleo, J. A. (2008). Developing Terrestrial-LiDAR-based digital elevation models for monitoring beach nourishment performance. Journal of Coastal Research, 24(6), 1555–1564.

Prokop, A. and Panholzer, H. (2009). Assessing the capability of terrestrial laser scanning for monitoring slow moving landslides. Natural Hazards and Earth System Science, 9(6), 1921–1928.

Rabatel, G., Gorretta, N., and Labb, S. (2011). Getting NDVI spectral bands from a single standard RGB digital camera: a methodological approach. Advances in Artificial Intelligence, 333-342.

Resop, J. P., and Hession, W. C. (2010). Terrestrial Laser Scanning for Monitoring Streambank Retreat: Comparison with Traditional Surveying Techniques. Journal of Hydraulic Engineering, 136(10), 794–798.

Sawaya, K. E., Olmanson, L. G., Heinert, N. J., Brezonik, P. L., and Bauer, M. E. (2003). Extending satellite remote sensing to local scales: land and water resource monitoring using high-resolution imagery. Remote sensing of Environment, *88*(1), 144-156.

Travelletti, J., & Oppikofer, T. (2008). Monitoring landslide displacements during a controlled rain experiment using a long-range terrestrial laser scanning (TLS). The International Archives of the Photogrammetry, Remote Sensing and Spatial Information Sciences, 37, 485-490.

DETAILED METHODS

Overview

During each April in 2014, 2015, and 2016, we collected both TLS and CRDP survey data of our point bar on White Clay Creek during a single-day field excursion. We selected our surveying schedule to limit the influence of dense summer-time vegetation while also capturing the result of winter/early spring flooding. In anticipation of our longitudinal project, we installed five concrete benchmarks (made of engraved aluminum disks pressed into wet concrete that was reinforced with steel rebar driven up to a meter into the subsurface to resist and prevent its disturbance) in early 2014, two on the upper bar and three on the cut bank side, to facilitate the alignment of repeated surveys over time. This section will provide further details on each surveying excursion and on our data processing methods. All TLS surveys were completed using a Trimble GX Advanced TLS. All quadcopter flights were flown in a random pattern to avoid pattern induced error that could occur with systematic, pre-programmed flights.

Year 1 Surveys

On April 11, 2014, TLS scanning of the entire study site was completed by positioning the instrument in seven different station locations throughout the area. Prior to scanning, white reference spheres were centered on the five aluminum benchmarks, with three additional spheres placed throughout the study area. All spheres were scanned at least once. This survey focused on the lower point bar where a high point density was obtained. The cut bank and intermediate bar were not the priority of this scan and only scanned partially. While the TLS survey was underway,

CRDP imagery of the study site were simultaneously collected. A GoPro Hero 2 sport camera was mounted to the underbelly of a QX3 350 quadcopter, parallel to the ground, and flown over the study area. The GoPro collected a 5 megapixel (MP) JPEG image every 5 seconds, totaling 144 RGB images looking down on the bar from above.

A large flood (6.2-year recurrence interval) affected the site in late April 2014, and to investigate its impacts, we collected a second TLS and CRDP survey on May 9, 2014 using the same equipment and survey design. This survey will not be included in this analysis; the interested reader is referred to Orefice, 2015.

Year 2 Surveys

The second TLS and CRDP surveying event was undertaken on April 16, 2015. Upon arrival to the site, it was discovered that the middle benchmark opposite bank (BM5, Figure 3) had been buried by overbank deposits and could not be found. White reference spheres were positioned on the remaining four benchmarks, with an additional four spheres placed throughout the area. TLS scanning was then performed at seven stations located throughout the site. The focus of this field campaign was again the lower point bar due to the observed active reorganization of sediment; the cut bank and upper bar was not surveyed in such detail. Two CRDP flights were collected while the TLS survey was underway. The first flight used a SJ4000 sport camera mounted to a QX3 350 quadcopter, collecting a 10 MP, low-compression JPEG every 3 seconds, totaling 220 RGB images. On the second flight, we substituted a modified SJ4000 sport camera, collecting a 10-MP low-compression JPEG of surface reflectance data in near-infrared wavelengths (Rabatel et al. 2011) every three seconds, for a total 220 NIRGB images.

Year 3 Surveys

In early January 2016, a large flood caused the root ball of a downed tree to become stuck on an older, partially buried log on the inside meander. The flood also scoured sediment around the upstream bar-side benchmark (BM2) and placed a large tire around the downstream bar-side benchmark (BM3). To ensure our ability to register future surveys to past surveys, three additional benchmarks (BM6, BM7, and BM8) were installed in March 2016. Their locations were chosen to avoid areas of active sediment reorganization, avoid overhead obstructions, attempt to replace threated benchmarks, and provide adequate spatial coverage over the study area. The additional benchmarks allow monitoring at this site to continue confidently into the future but they introduce position uncertainty and registration difficulties because they are not observable in the 2014 or 2015 surveys.

The third TLS and CRDP surveying event was undertaken on April 16, 2016. The TLS field campaign attempted a fully continuous survey over the point bar, upper bar, and cut bank by scanning from seven locations and including six benchmarks with four spheres located throughout the study area. This field campaign surveyed a larger area that previous campaigns by completing 360 degree scans from all locations. Whereas the previous survey's restricted viewshed focused solely on the lower bar. Two CRDP imagery flights were collected just prior to TLS surveying. The first flight used a Xiaomi YI sport camera with a fixed focus lens intended for subjects less than 5 meters from the lens. To account for the flying altitude of 40 meters, we manually refocused the lens so that the subject in focus was now 40 meters away (Liang, 2016). Using the adjusted camera, we collected 92 RGB JPEG images at 16MP resolution. The second flight used a SJ4000 sport camera with a Blu 22 filter installed (Rabatel et al., 2011) which filters blue wavelengths and allows NIR wavelengths to be captured

on the normal blue band. As this second flight neared completion, user error caused the quadcopter to collide with a tree on the opposite bank. During collision, the camera was dislodged from its mount and lost to the woodland creatures in the dense underbrush. On April 18, 2016 at approximately 11:00 am, a third CRDP imagery flight was performed with an SJ4000 sport camera modified by IR Pro to collect NIR imagery, collecting 200 NIRGB, JPEG images at 11 MP resolution.

Data Product Creation

TLS Data Output and Manipulation

For each of the three years, the following raw point data processing procedure was followed. Each TLS scan location was recorded as an individual .ppl with embedded sphere numbers and locations. Realworks (Trimble) assigned fixed numbers to the white reference spheres, which are used to automatically align all scans. For each year's imagery, the separate-station scans from a surveying event were aligned with RMSE less than 0.01m. The project was then saved as a .rwp and the point cloud exported as a .txt file with ten columns: X, Y, Z, Nx, Ny, Nz, Intensity, Red, Green, and Blue. The point clouds are contained within a Cartesian coordinate system where (0,0,0) is the X, Y, Z position of the scanner at the first scanning station and all recorded points emanate radially from that origin. We note that each year's TLS survey data generated its own Cartesian coordinate system, independent of any other survey event.

To compare annual changes, the separate, annual TLS point clouds were registered in the same coordinate system. Geo-referencing point clouds into real world coordinate systems, which would facilitate systematic comparison among annual

40

surveys, is known to create systematic positional errors on the order of a few centimeters (Lichit, 2005; Coveney and Steward Fotheringham, 2011). To reduce error propagation through our time-series of observations, we instead registered point clouds relative to each other, specifically registering the 2015 and 2016 TLS point clouds into the 2014 Cartesian coordinate system using open-source point-cloud editing software (Cloud Compare). In our co-registration approach, we identified the benchmarks in each annual scene and assigned them same coordinates. This resulted in a positional RMSE of less than 0.01m for both the 2015 and 2016 point clouds with respect to the 2014 point cloud.

CRDP Data Outputs and Manipulation

We describe herein a reliable and repeatable processing method we developed and used for all datasets using AGI Photoscan Pro software. Our first attempts to generate a surface model included every image collected and limited ground control points (GCP's): white reference spheres or stationary objects (large rocks, large logs, base of trees, spheres not located on benchmarks, etc…). The resultant CRDP-based DEMs appeared to accurately represent the study area at first approximation and with acceptable reported positional errors, and matched TLS data sets well around GCPs and in map view (X and Y axis). However, the CRDP models were severely warped when compared to TLS-based DEMs, with displacements of up to +/- 0.50m vertically in cross section (Z axis) between GCP's. We achieved significant improvements in agreement between TLS and CRDP surface models, while still retaining acceptable positional errors, by including 15-20 GCPs and recursive photo inclusion (both described in the next section) until the model error and shape stabilized.

Recursive Photo Inclusion Workflow

  Ten images were initially selected based on their complete view of the bar, inclusion of GCPs, and approximate equidistant spacing between images. These images were aligned using High alignment, disabled pair preselection, 4,000 key points, and unlimited tie points (Morgan et al., 2017; AGI, 2016) these settings were used in all subsequent alignments. Five benchmarks were identified in the images and labeled as BM1-BM5; these were added manually as control points to the images. An additional 10 stationary objects (large rocks, large logs, base of trees, spheres not located on benchmarks, etc…) identified on the bar's surface and located in all images, were used as control points. The CRDP scenes were manually aligned to that year's TLS survey by assigning in Photoscan's reference pane the TLS Cartesian coordinates of each benchmark and as many of the identified GCPs as possible, and re-aligning the scene. Photoscan's user manual recommends (AGI, 2016) an additional calibration step to correct for lens distortions using AGI's Lens calibration procedure; however, due to the camera lens' short focal length, the calibration grid produced by AGI Lens could not fill the entire image frame. Improved calibration was achieved using GCP coordinates to calibrate the images in Photoscan's "Camera Calibration" tool with fx, fy, cx, cy, p1, p2, … selected as per AGI recommendations (AGI, 2016). Once calibrated, the projected images were re-aligned a final time, with an AGI reported positional error of 0.22M. Next, another ten images were selected to fill spatial gaps not covered by the original ten. In these new ten images, the benchmarks and stationary objects were identified; using the same TLS-based Cartesian alignment protocol as before, the images were aligned, calibrated, and aligned again with reported positional error around 0.12M. Additional images were added to the scene in the same manner, recursively, for a total of 30 images (positional error = 0.08m), then

40 images (positional error = 0.05m), then. 45 images (positional error = 0.04m). Next, we creating a triangular mesh in Photoscan Pro using the "High" facet setting and overlaid an image mosaic to create the final 0.1M ortho-rectified areal image used for processing. That ortho-image and final raw dense cloud were exported for further analyses. The 2015 and 2016 RGB and NIR photoscan projects were processed similarly, using each year's respective TLS scan, which themselves had been georeferenced into the established 2014 coordinate system.

In summary, our data flow yielded the following products, all in the same coordinate system -- 2014: TLS point cloud, CRDP point cloud, RGB orthomosaic; 2015: TLS point cloud, CRDP point cloud, RGB orthomosaic, NIRGB orthomosaic. 2016: TLS point cloud, CRDP point cloud, RGB orthomosaic, NIRGB orthomosaic.

In comparing point clouds, we noticed a further challenge into the analysis: how should we compare two surveys of the same object, but taken at different times, where resultant point density (resolution) and exact point location (accuracy) are similar, but not identical to smooth these inter-year positional disagreements, we generated a raster, overlaying each point cloud with a 0.10m square grid; every point that fell within the X and Y coordinates of a particular grid cell was assigned to that cell. Descriptive statistics (minimum elevation, maximum elevation, range of elevation, standard dev of elevation, and point density) could then be calculated on the column of points that occurred within each cell.

<center>Classification</center>

During our analysis, we noticed important differences in how landcover types were sensed by the two techniques. We thus performed a spatial classification of landcover type to facilitate analyses that quantify how detected regions of bare earth,

<center>43</center>

dry vegetation, and green vegetation influence topographic measurements over the course of multiple annual surveys. NIR imagery, collected in 2015 and 2016 (but not 2014), provided raw data to detect live vegetation on the landscape, thus facilitating a rapid, robust, and unbiased classification of landcover type. Under ideal circumstances, vegetation type and health could be discriminated via the normalized difference vegetation index (NDVI). Unfortunately, due to the 2016 NIR being collected on a different day and at a different time of day that the RGB, the place and distribution of shadows differ between orthophotos of that year. To remove shadows, the RGB ortho image was band-ratioed using R/G, R/B, and B/G, while the NIRGB was band-ratioed in NIR/B and NIR/G. The five band ratios were stacked in ENVI and a supervised classification of 4 classes (water, bare earth, green vegetation, and dry vegetation) was performed. While the 2015 data could facilitate NDVI analyses, the same procedure that was used on the 2016 orthoimage was performed on the 2015 orthoimage to remain consistent.

2014 could not be classified using this technique because NIR was not collected. Although future analyses might be able to use a similar procedure to differentiate bare earth from non-bare earth and then manually classify the water areas so that 2014 could be partially included in analyses.

DEM Generation

Raw point clouds directly exported from each method's processing software were turned into 10cm DEM's with summary statistics (point density, minimum elevation, average elevation, standard deviation of elevation, and elevation range) calculated from the raw points falling within the X-Y coordinates of each cell. Each

cell was assigned to a single landcover type as previously described. The minimum

elevation was used as the elevation value for all DEMs.

Appendix B

TYPOGRAPHIC AREAS
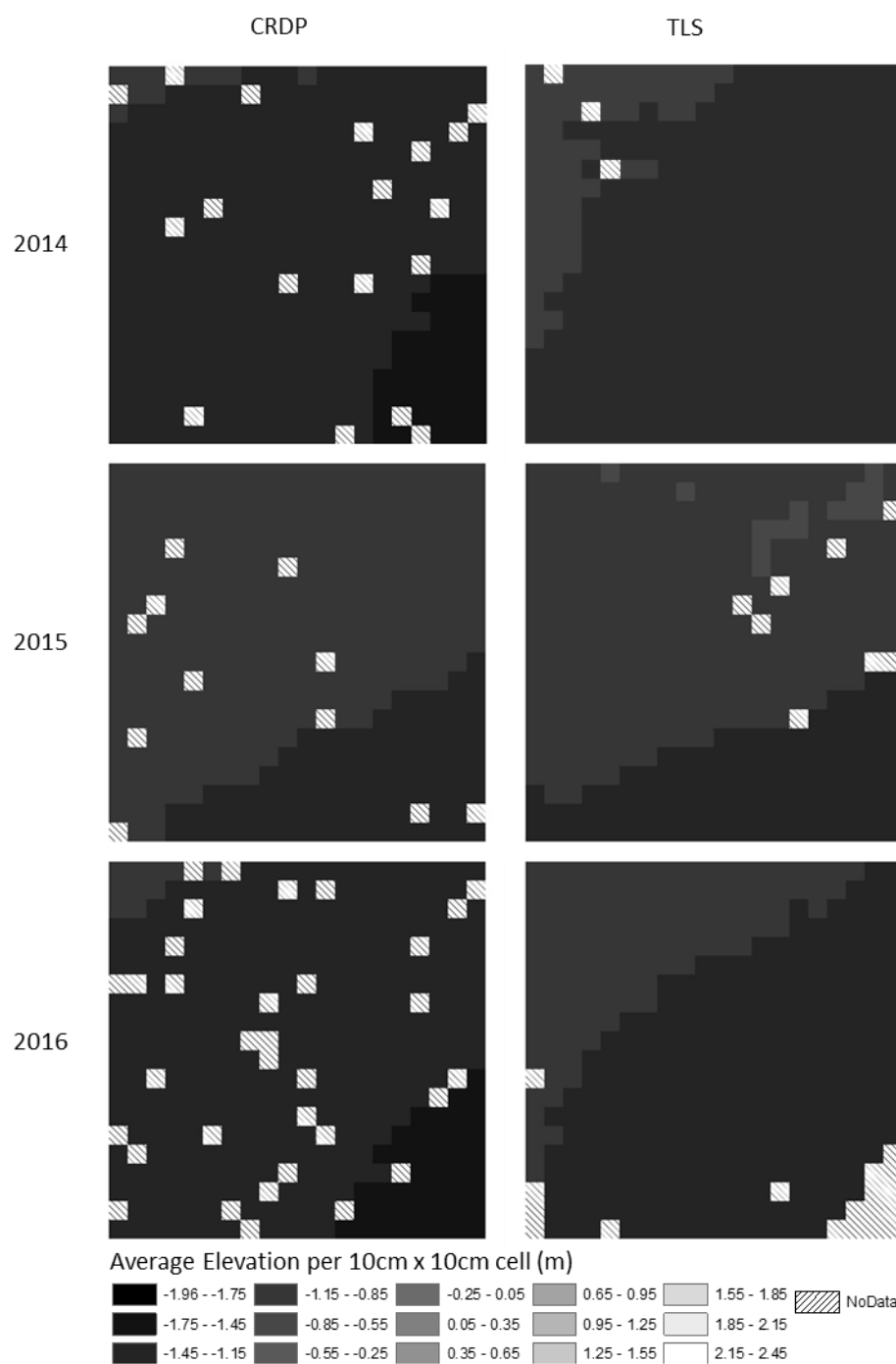
Figure 8   Comparing average elevation change between CRDP and TLS 10cm
               DEM's in typographic area 1 (sand to gravel). Small study areas are 2
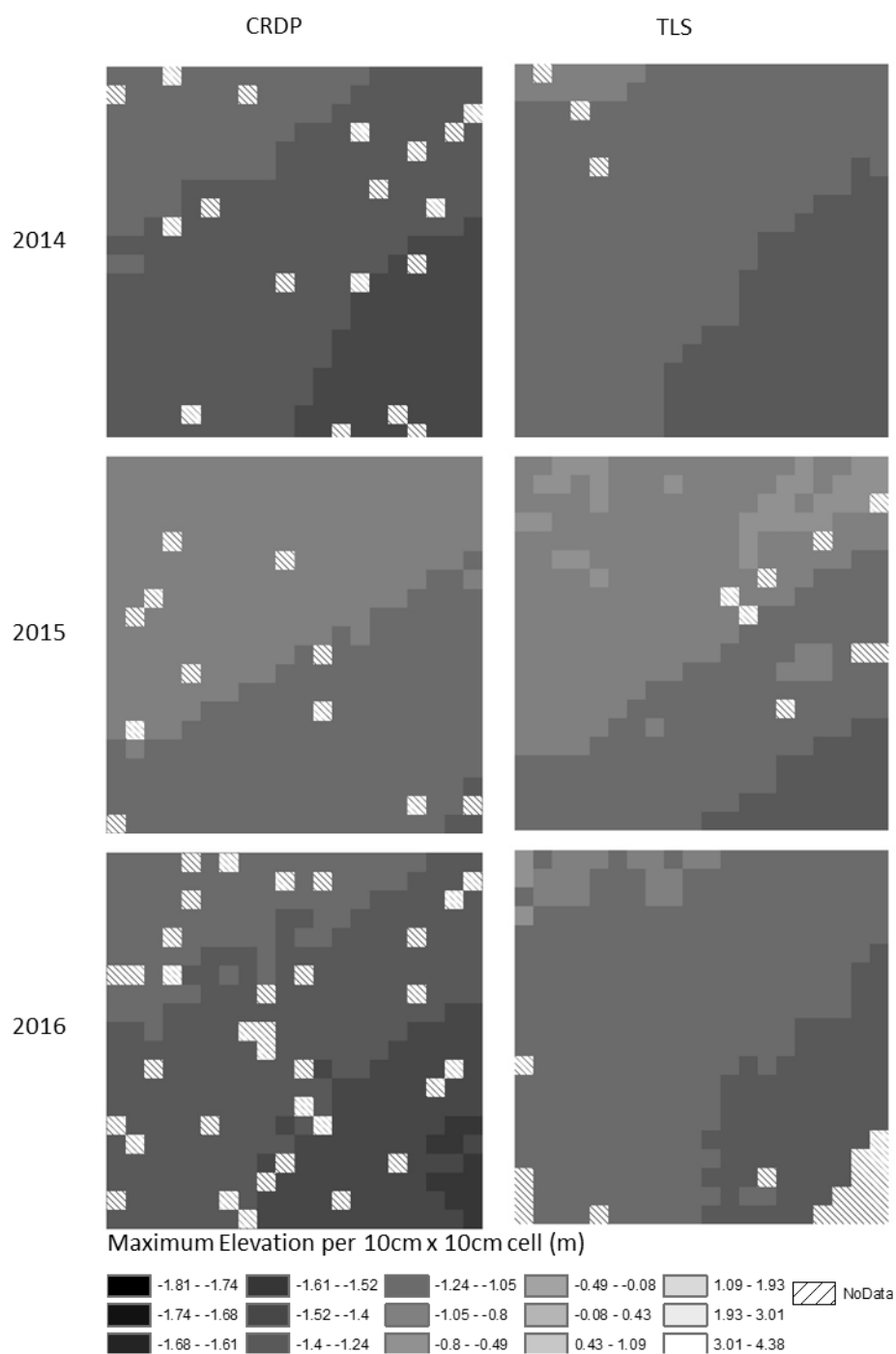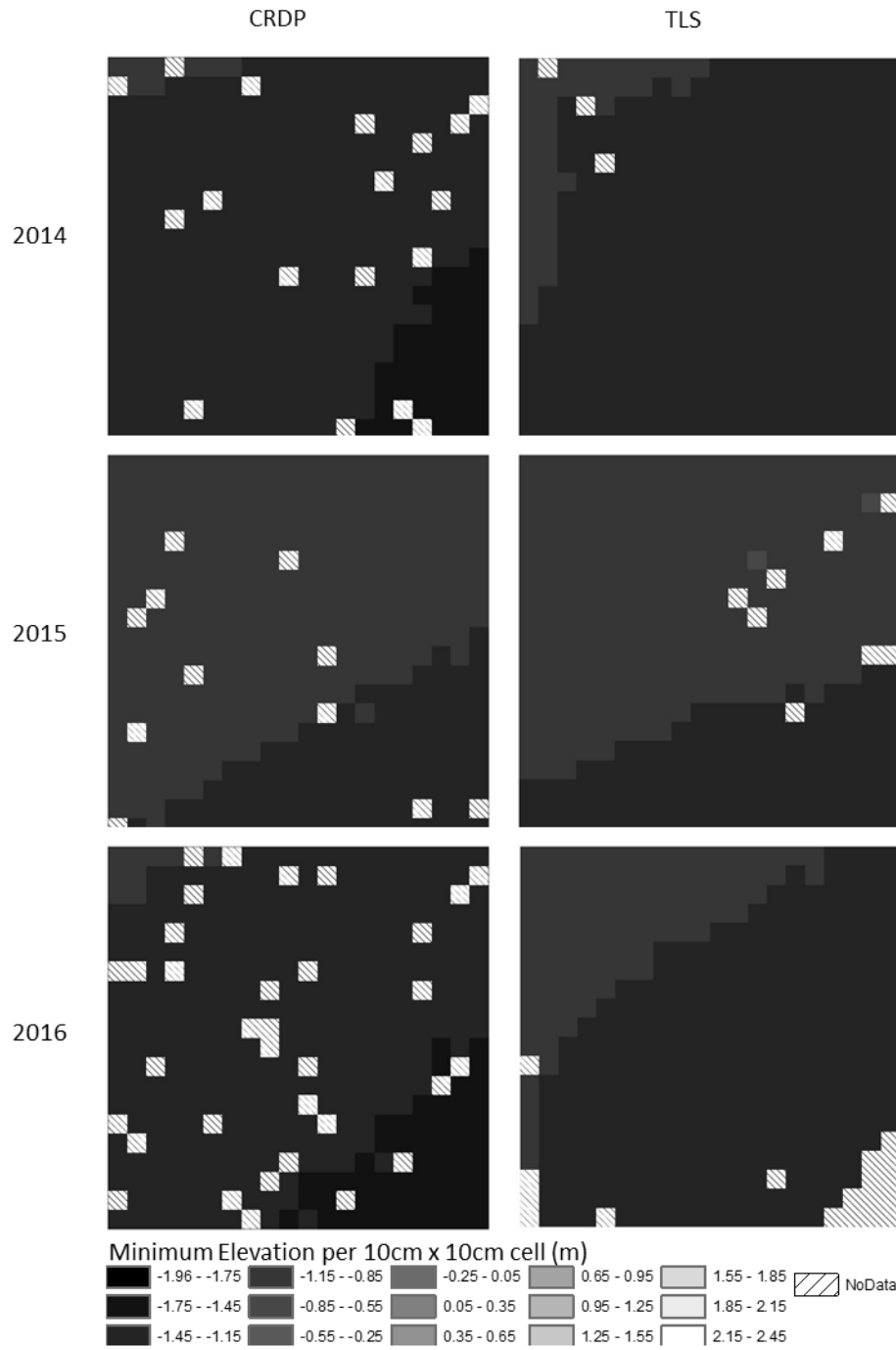   meters long per side.

CRDP   TLS

2014

2015

2016

Maximum Elevation per 10cm x 10cm cell (m)

-1.81 - -1.74	-1.61 - -1.52	-1.24 - -1.05	-0.49 - -0.08	1.09 - 1.93	NoData
-1.74 - -1.68	-1.52 - -1.4	-1.05 - -0.8	-0.08 - 0.43	1.93 - 3.01	
-1.68 - -1.61	-1.4 - -1.24	-0.8 - -0.49	0.43 - 1.09	3.01 - 4.38	

Figure 9   Comparing maximum elevation between CRDP and TLS 10cm DEM's in typographic area 1 (sand to gravel). Small study areas are 2 meters long per side.

Figure 10   Comparing minimum elevation between CRDP and TLS 10cm DEM's in typographic area 1 (sand to gravel). Small study areas are 2 meters long per side.
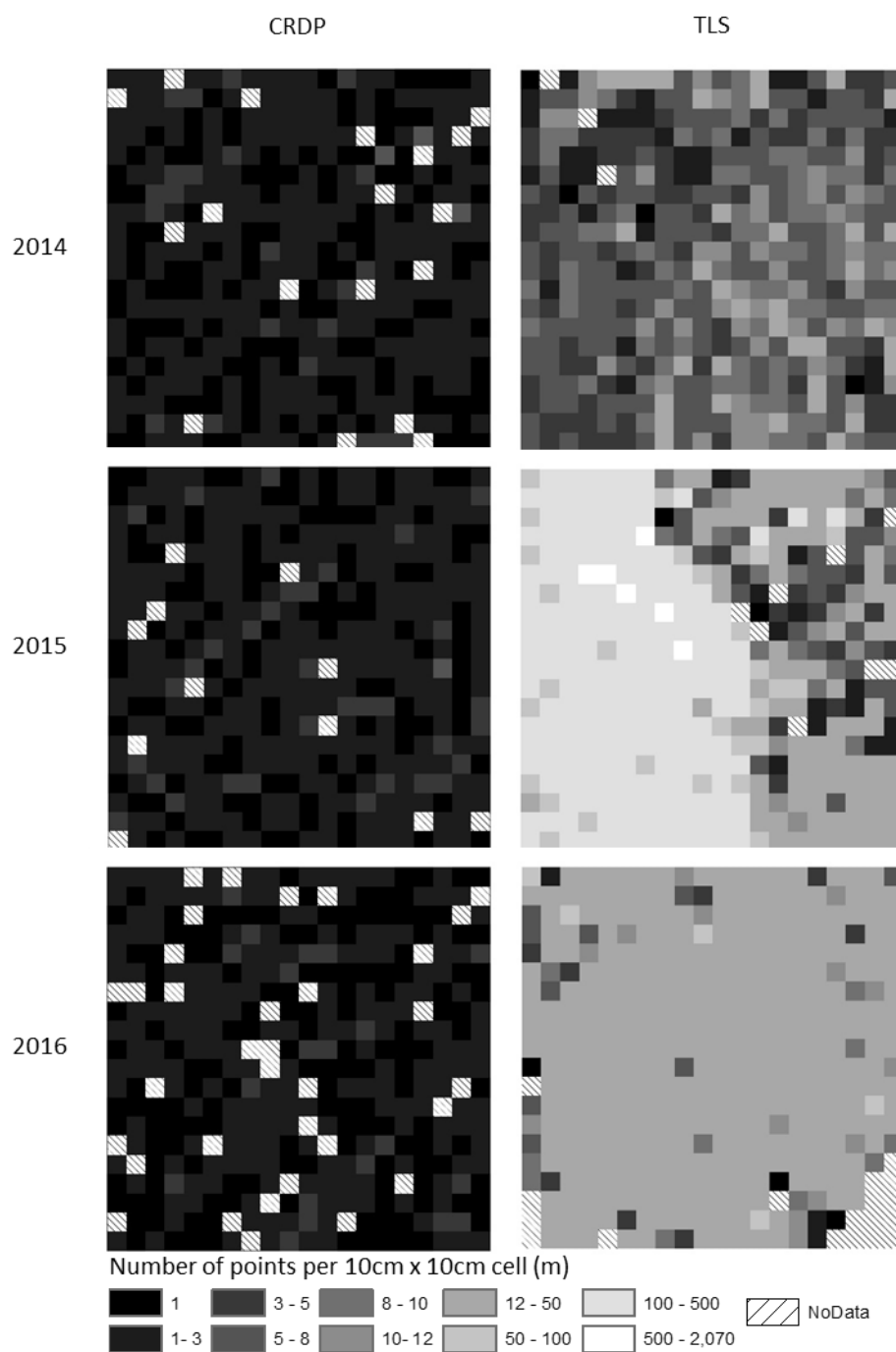
Figure 11   Comparing point density between CRDP and TLS 10cm DEM's typographic area 1 (sand to gravel). Small study areas are 2 meters long per side.
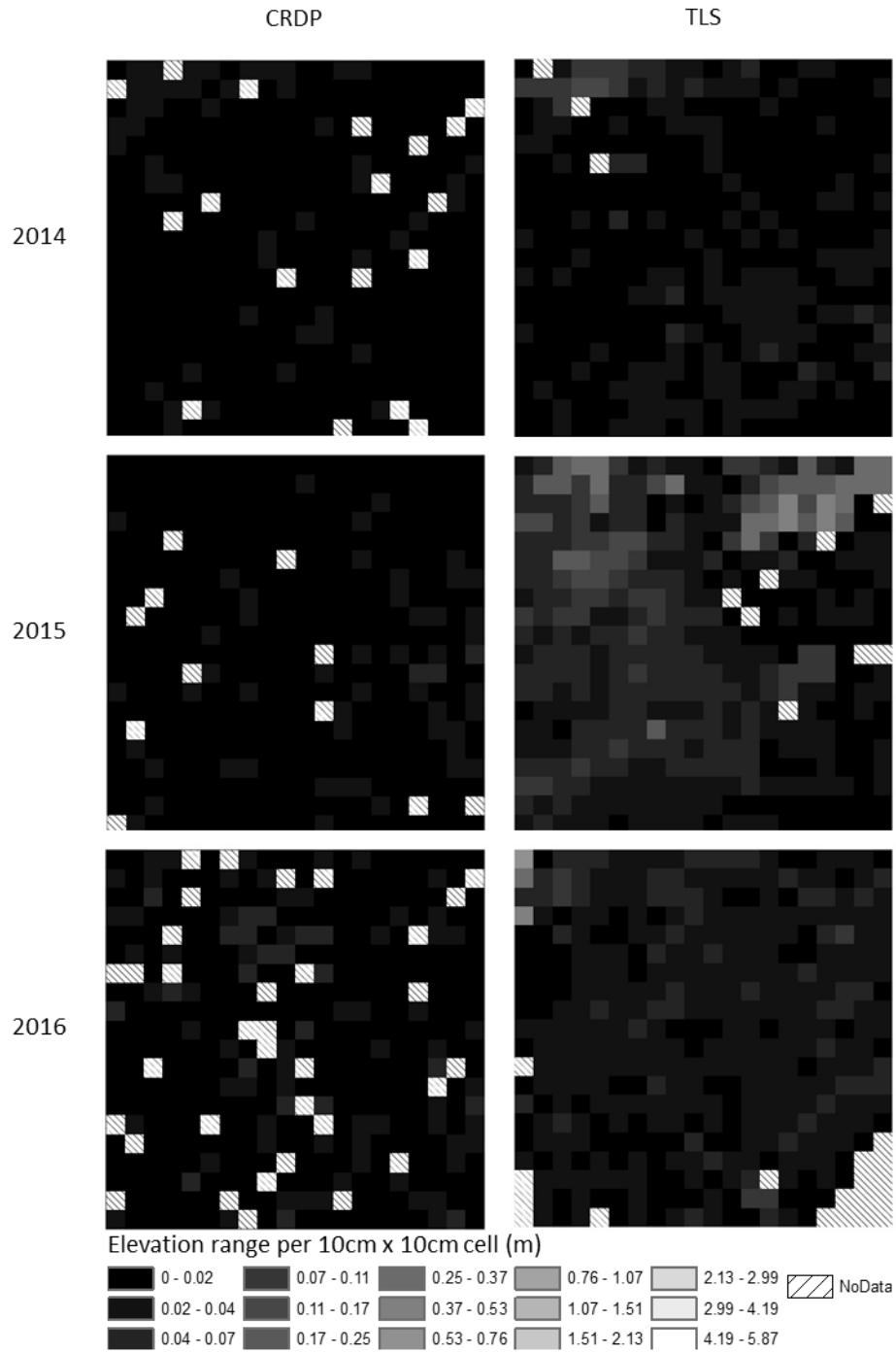
Figure 12   Comparing range of elevation points between CRDP and TLS 10cm
DEM's in typographic area 1 (sand to gravel). Small study areas are 2
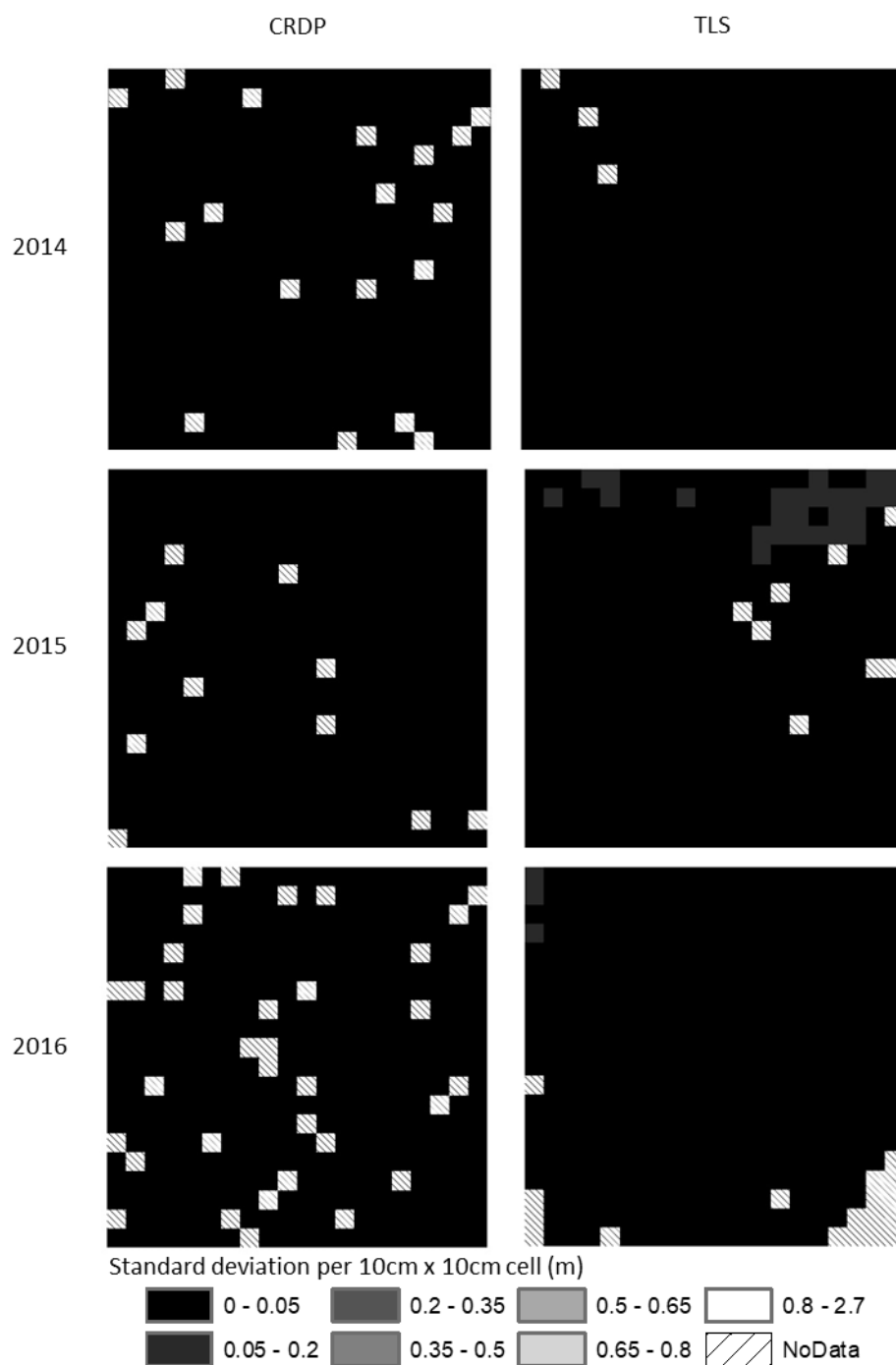meters long per side.

Figure 13   Comparing standard deviation of points between CRDP and TLS 10cm
             DEM's in typographic area 1 (sand to gravel). Small study areas are 2
             meters long per side.
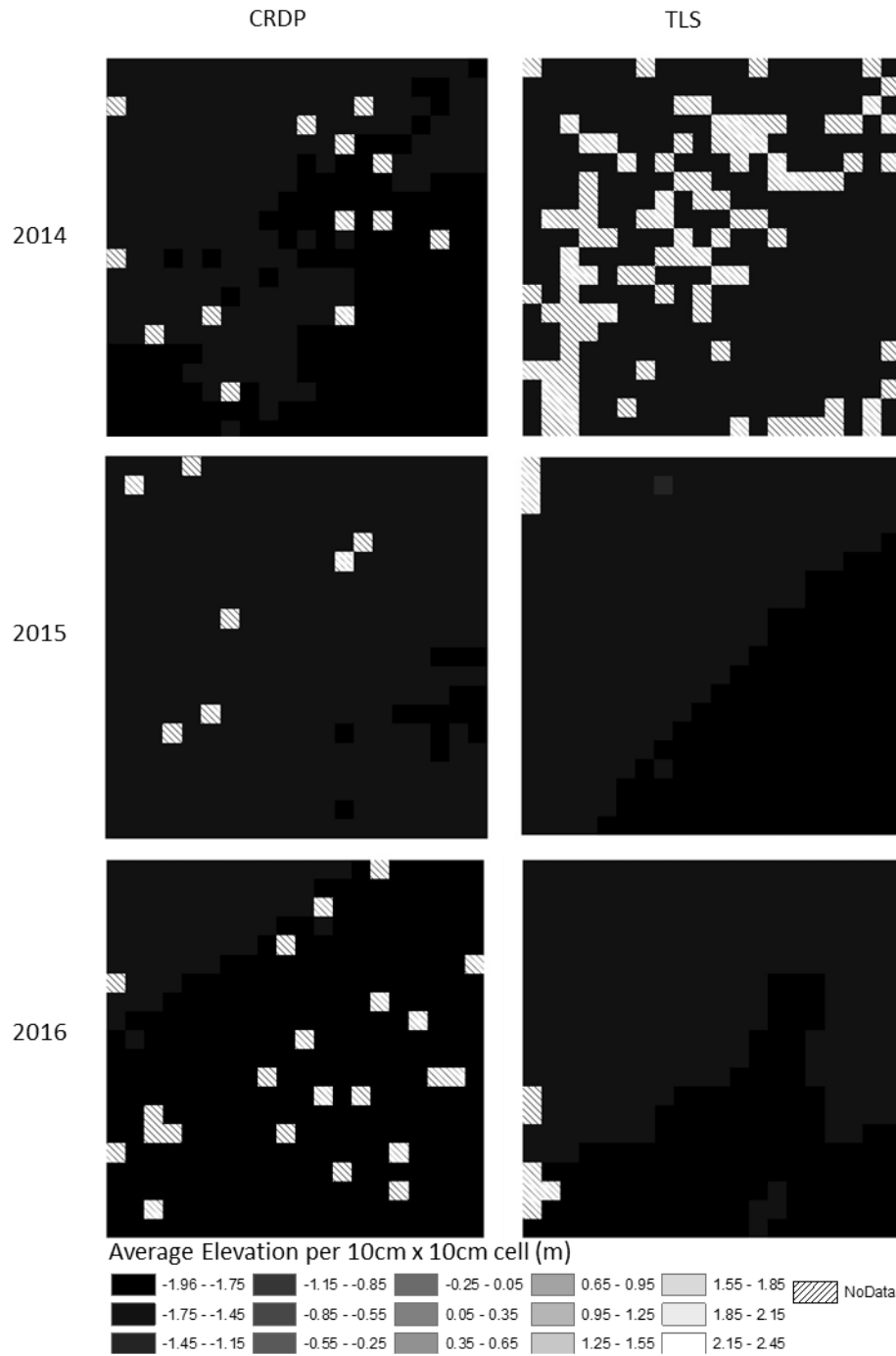
Figure 14   Comparing average elevation change between CRDP and TLS 10cm
            DEM's in typographic area 2 (mud to sand). Small study areas are 2
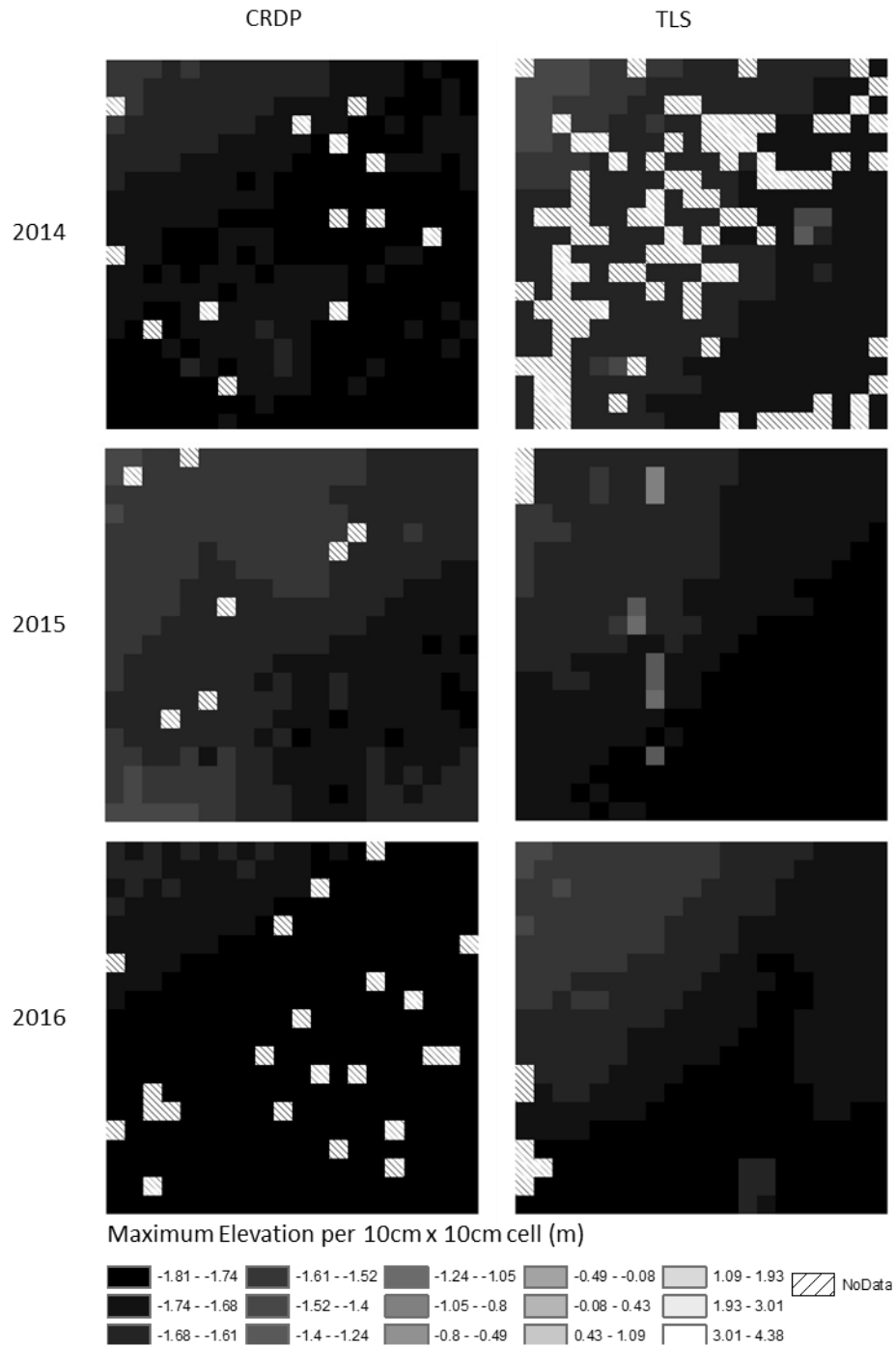   meters long per side.

Maximum Elevation per 10cm x 10cm cell (m)

-1.81 - -1.74	-1.61 - -1.52	-1.24 - -1.05	-0.49 - -0.08	1.09 - 1.93	NoData
-1.74 - -1.68	-1.52 - -1.4	-1.05 - -0.8	-0.08 - 0.43	1.93 - 3.01	
-1.68 - -1.61	-1.4 - -1.24	-0.8 - -0.49	0.43 - 1.09	3.01 - 4.38	

Figure 15   Comparing maximum elevation between CRDP and TLS 10cm DEM's in typographic area 2 (mud to sand). Small study areas are 2 meters long per side.
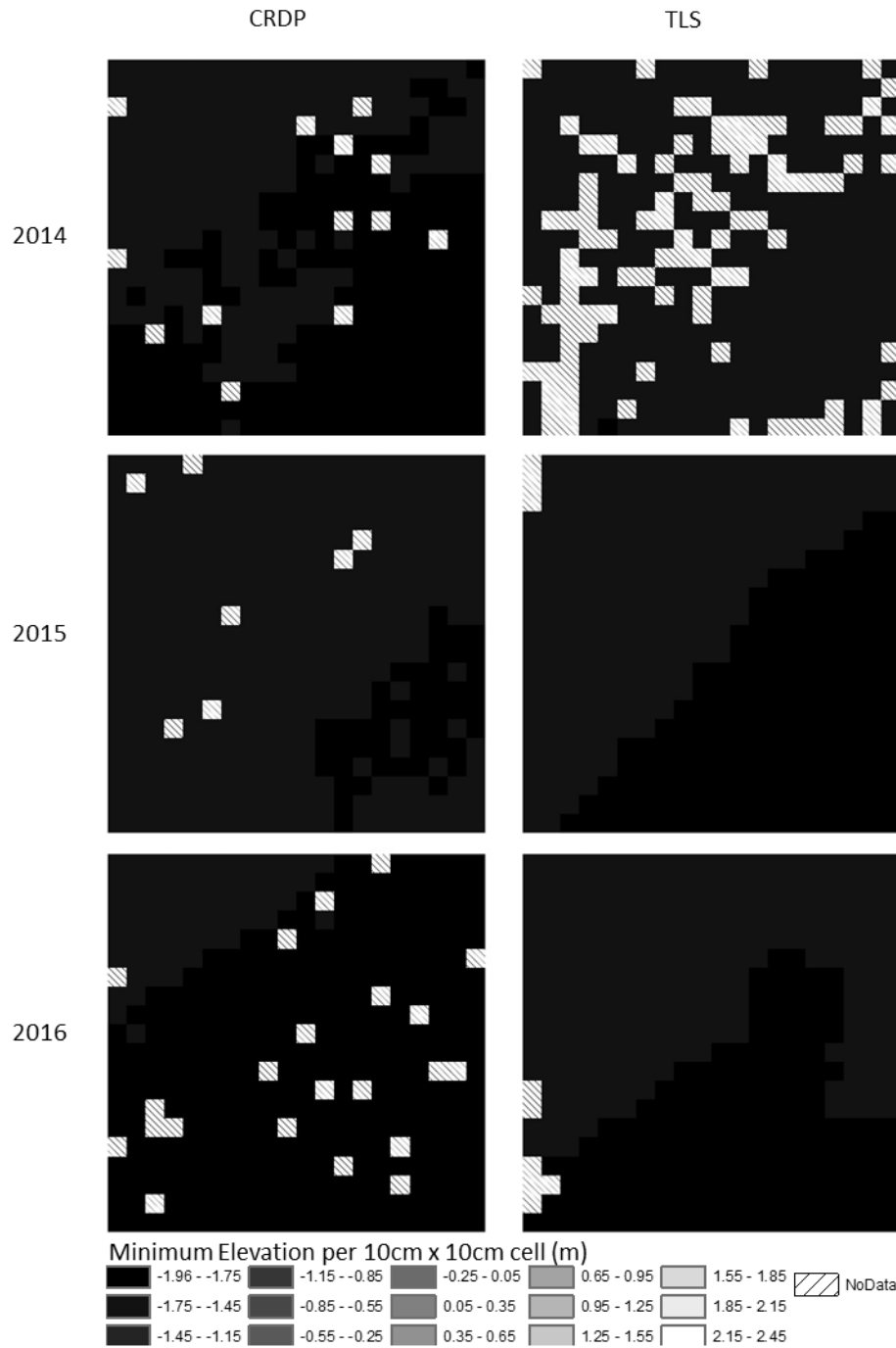
Figure 16   Comparing minimum elevation between CRDP and TLS 10cm DEM's in typographic area 2 (mud to sand). Small study areas are 2 meters long per side.
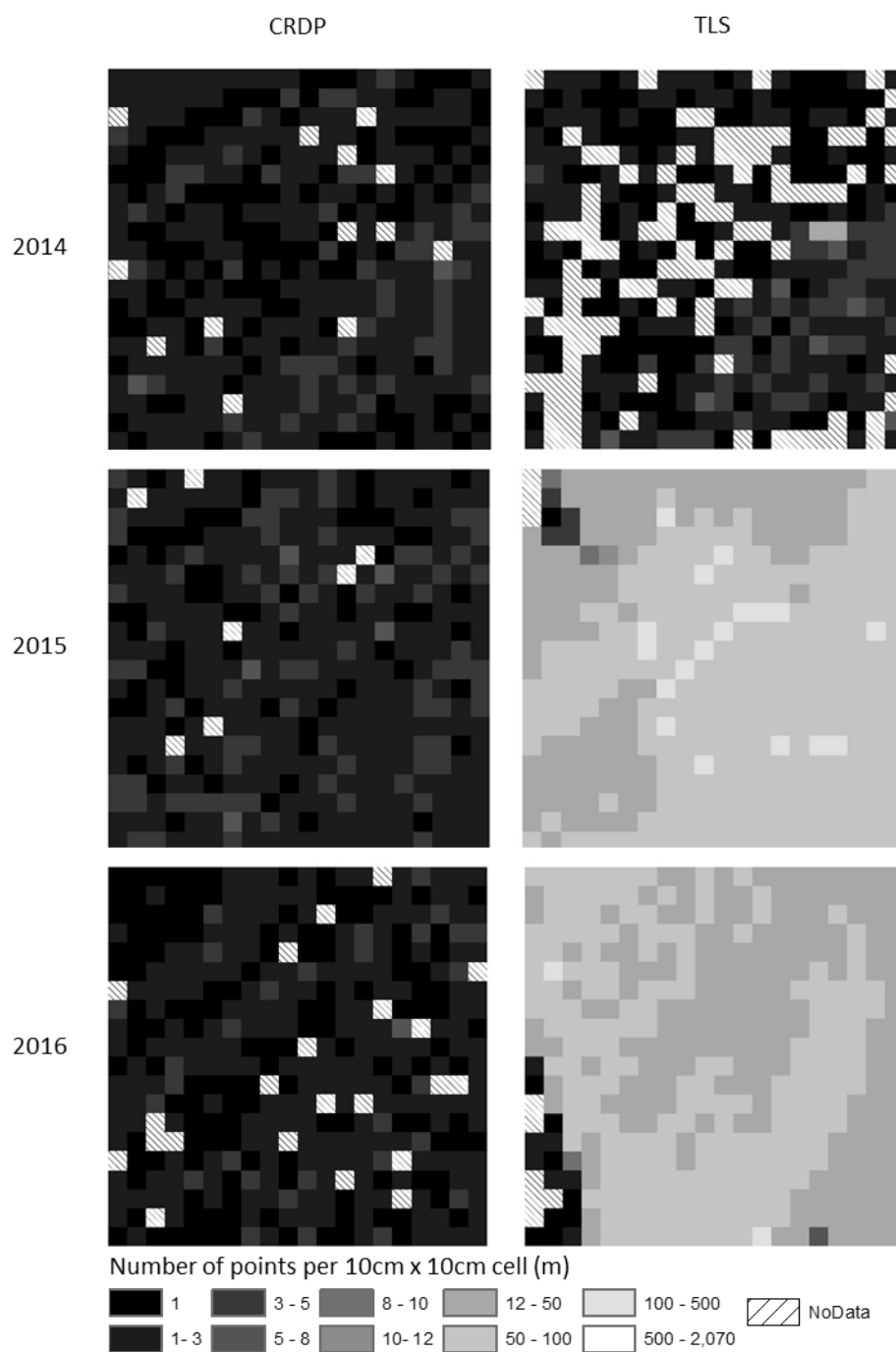
	CRDP	TLS
2014		
2015		
2016		

Number of points per 10cm x 10cm cell (m)

■ 1	■ 3 - 5	■ 8 - 10	■ 12 - 50	□ 100 - 500	▨ NoData	
■ 1- 3	■ 5 - 8	■ 10- 12	■ 50 - 100	□ 500 - 2,070		

Figure 17   Comparing point density between CRDP and TLS 10cm DEM's in typographic area 2 (mud to sand). Small study areas are 2 meters long per side.
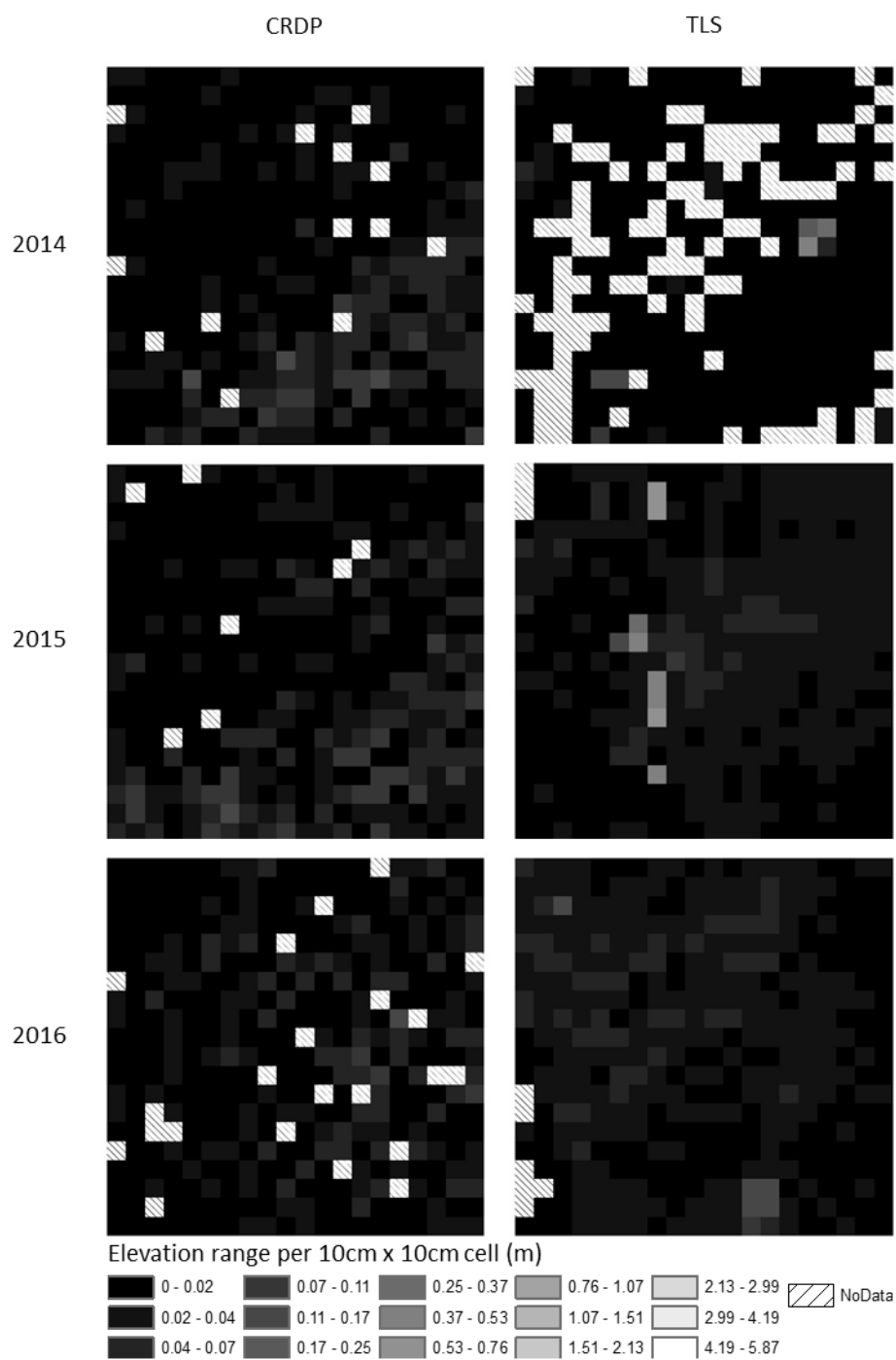
Figure 18   Comparing range of elevation points between CRDP and TLS 10cm
DEM's in typographic area 2 (mud to sand). Small study areas are 2
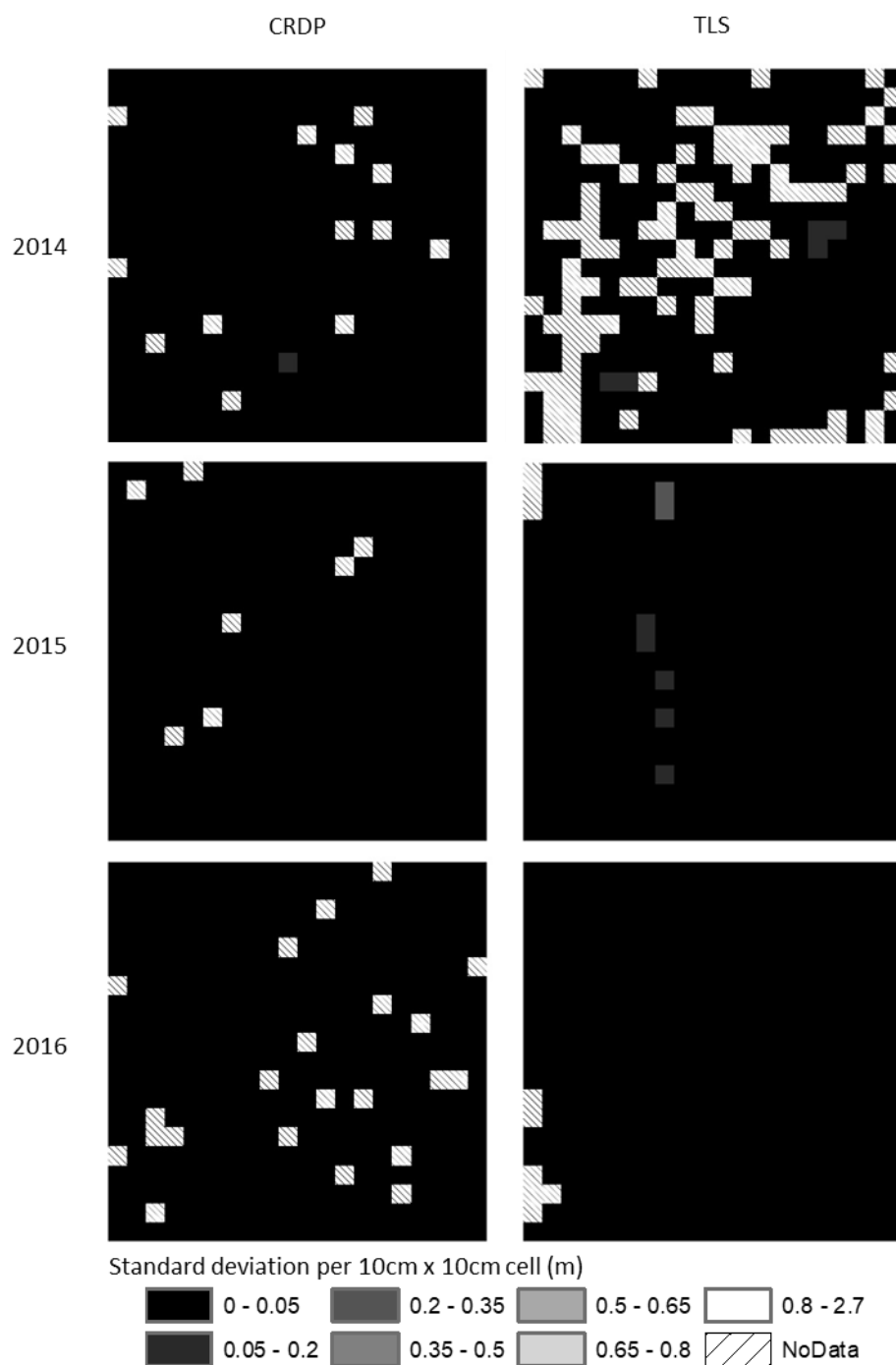meters long per side.

Figure 19   Comparing standard deviation of points between CRDP and TLS 10cm
              DEM's in typographic area 2 (mud to sand). Small study areas are 2
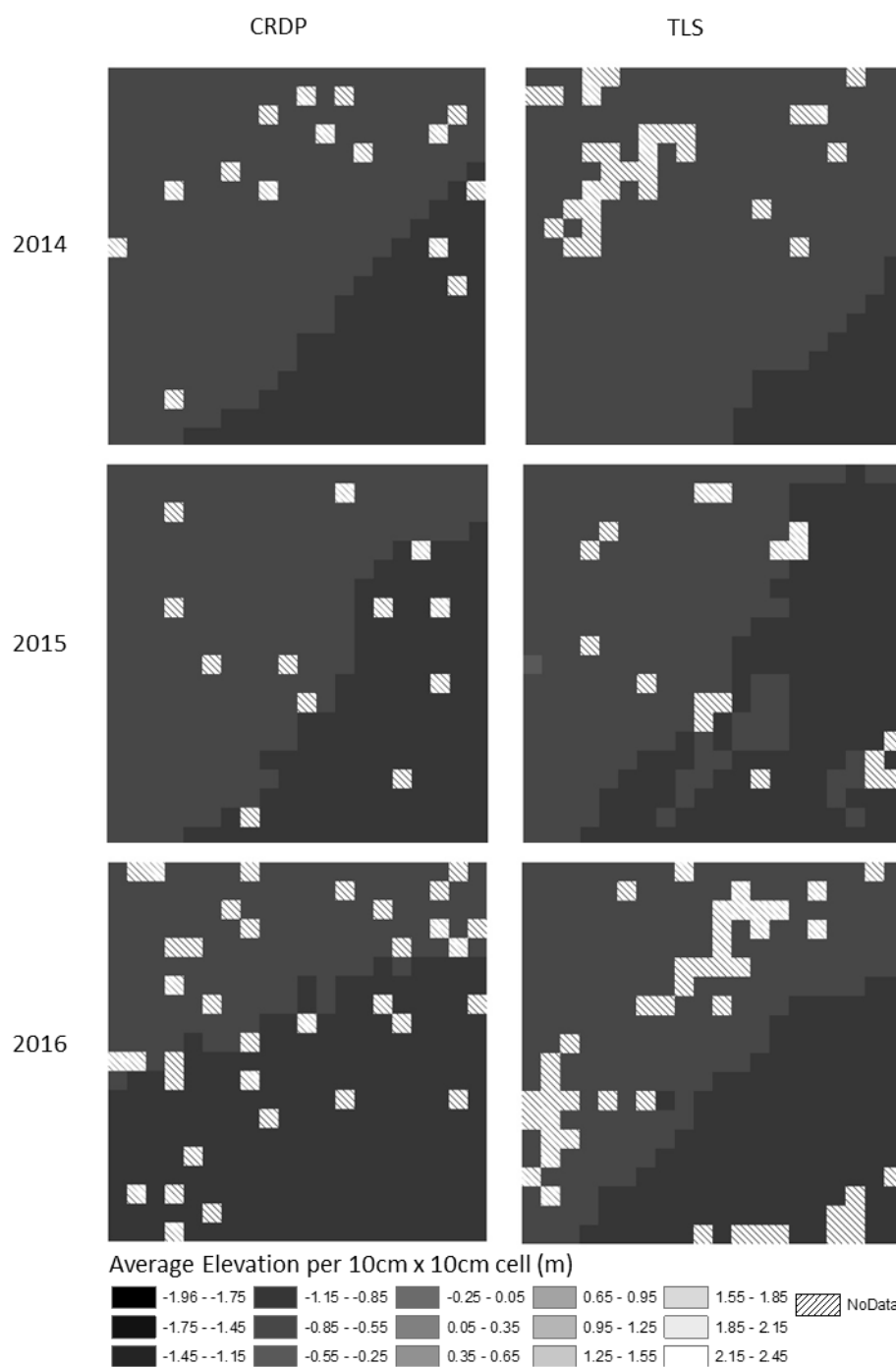   meters long per side.

Figure 20   Comparing average elevation change between CRDP and TLS 10cm
            DEM's in in typographic area 3 (Groundcover and grasses). Small study
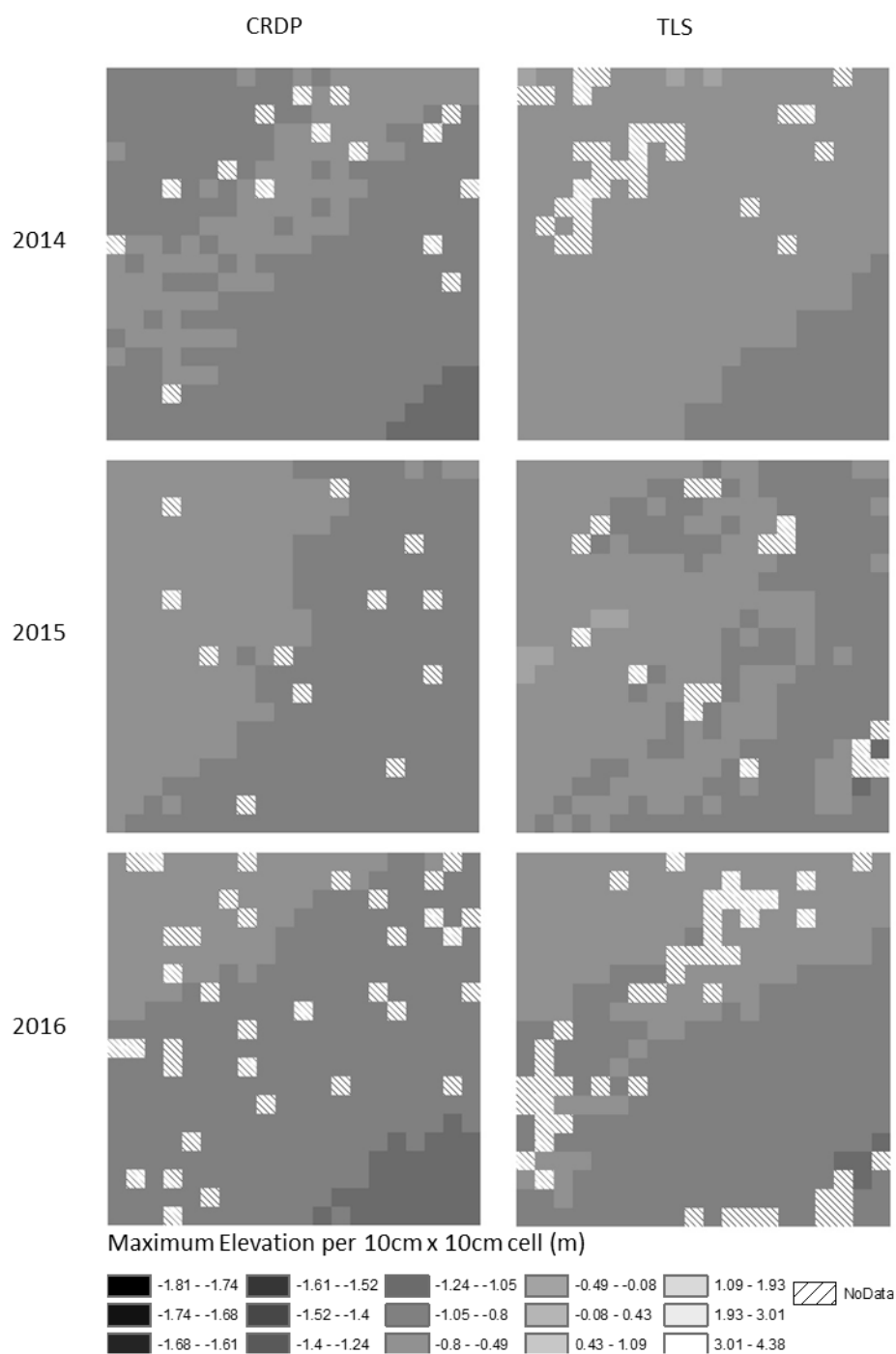   areas are 2 meters long per side.

Figure 21   Comparing maximum elevation between CRDP and TLS 10cm DEM's in typographic area 3 (ground cover and grasses). Small study areas are 2 meters long per side.
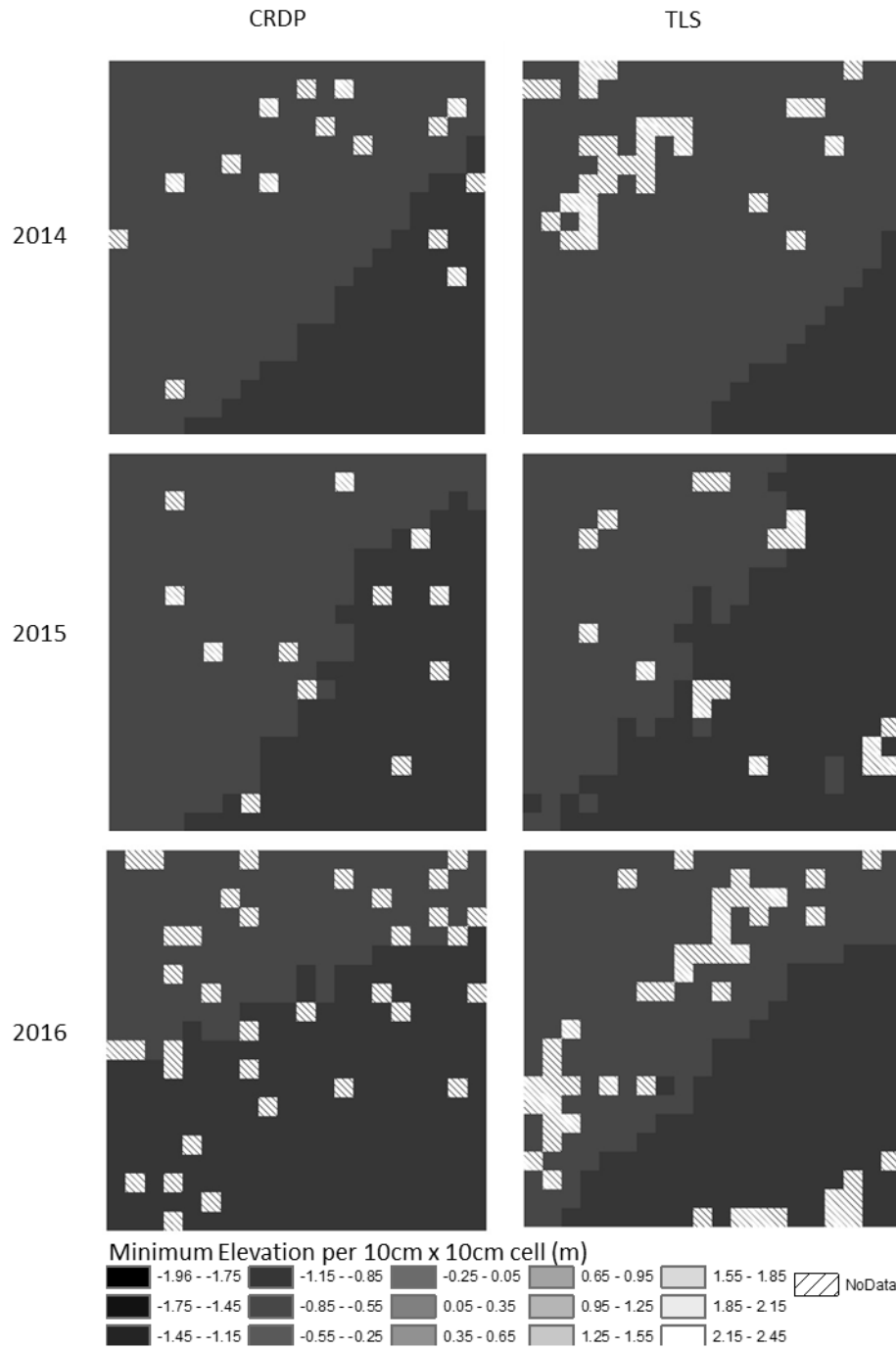
CRDP | TLS

2014

2015

2016

Minimum Elevation per 10cm x 10cm cell (m)

-1.96 - -1.75	-1.15 - -0.85	-0.25 - 0.05	0.65 - 0.95	1.55 - 1.85	NoData
-1.75 - -1.45	-0.85 - -0.55	0.05 - 0.35	0.95 - 1.25	1.85 - 2.15	
-1.45 - -1.15	-0.55 - -0.25	0.35 - 0.65	1.25 - 1.55	2.15 - 2.45	

Figure 22   Comparing minimum elevation between CRDP and TLS 10cm DEM's in typographic area 3 (ground cover and grasses). Small study areas are 2 meters long per side.

CRDP   TLS

2014

2015

2016

Number of points per 10cm x 10cm cell (m)

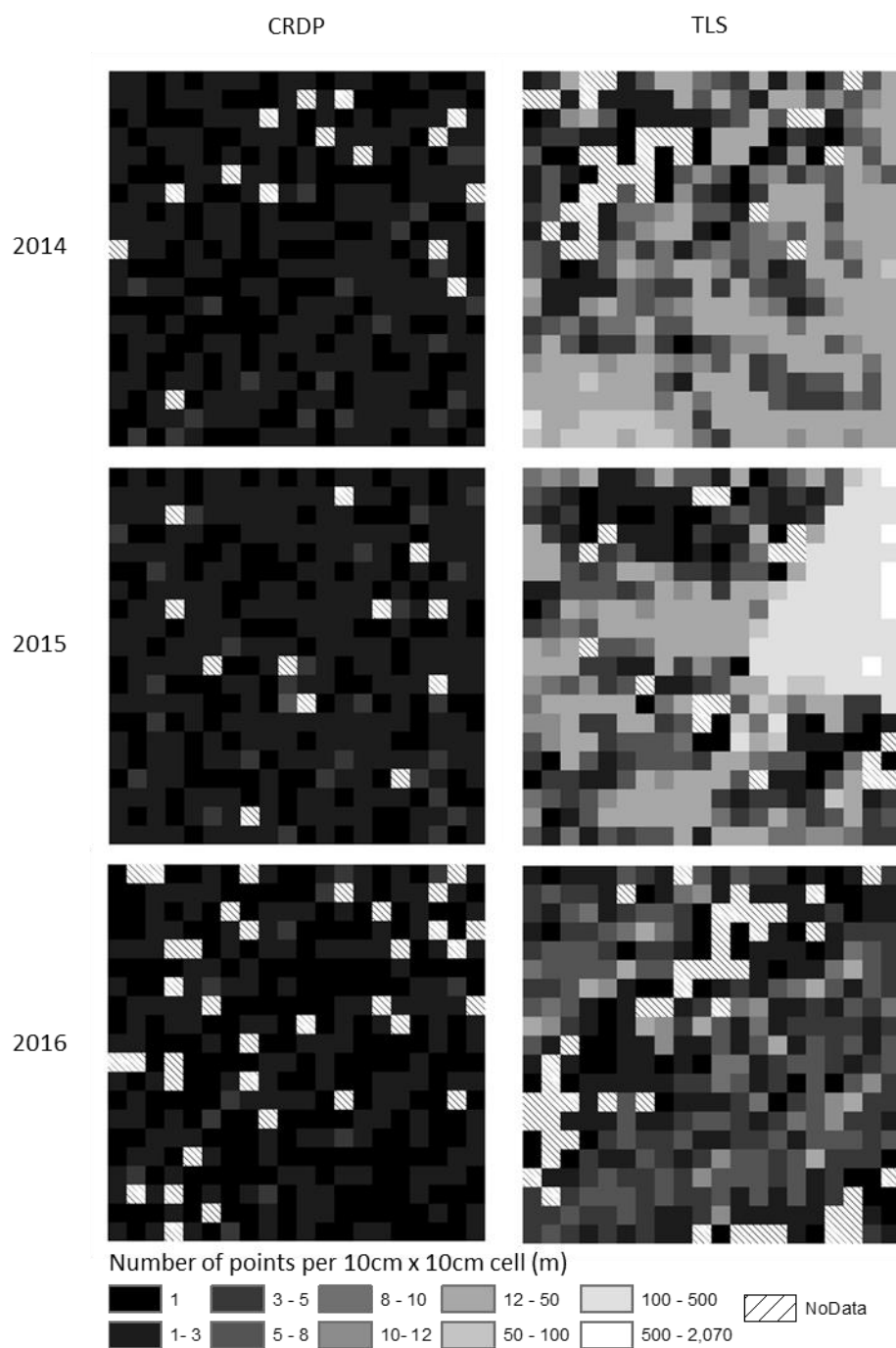| 1 | 3 - 5 | 8 - 10 | 12 - 50 | 100 - 500 | NoData |
| 1- 3 | 5 - 8 | 10- 12 | 50 - 100 | 500 - 2,070 | |

Figure 23   Comparing point density between CRDP and TLS 10cm DEM's in typographic area 3 (ground cover and grasses). Small study areas are 2 meters long per side.
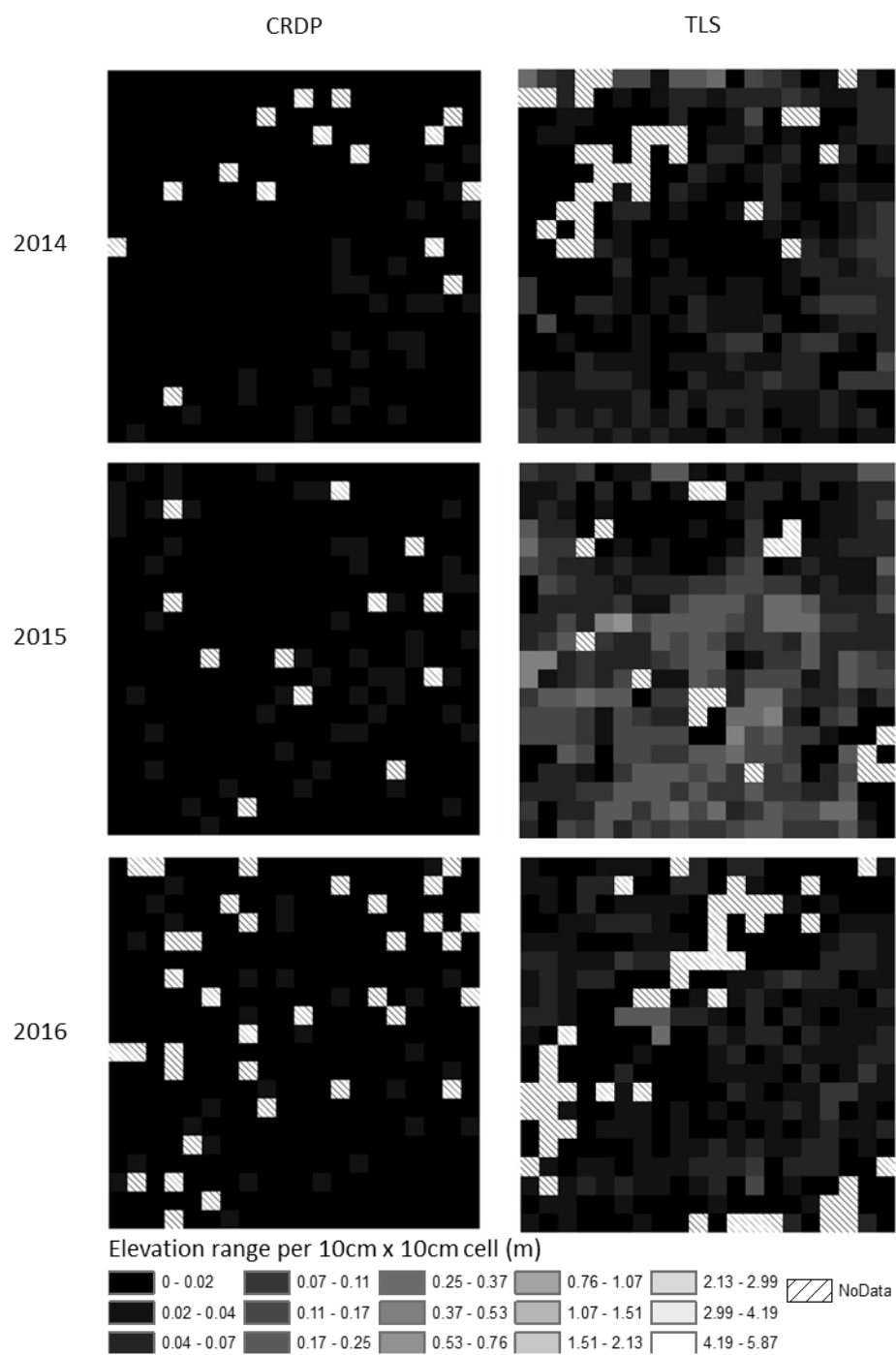
Figure 24   Comparing range of elevation points between CRDP and TLS 10cm
            DEM's in typographic area 3 (ground cover and grasses). Small study
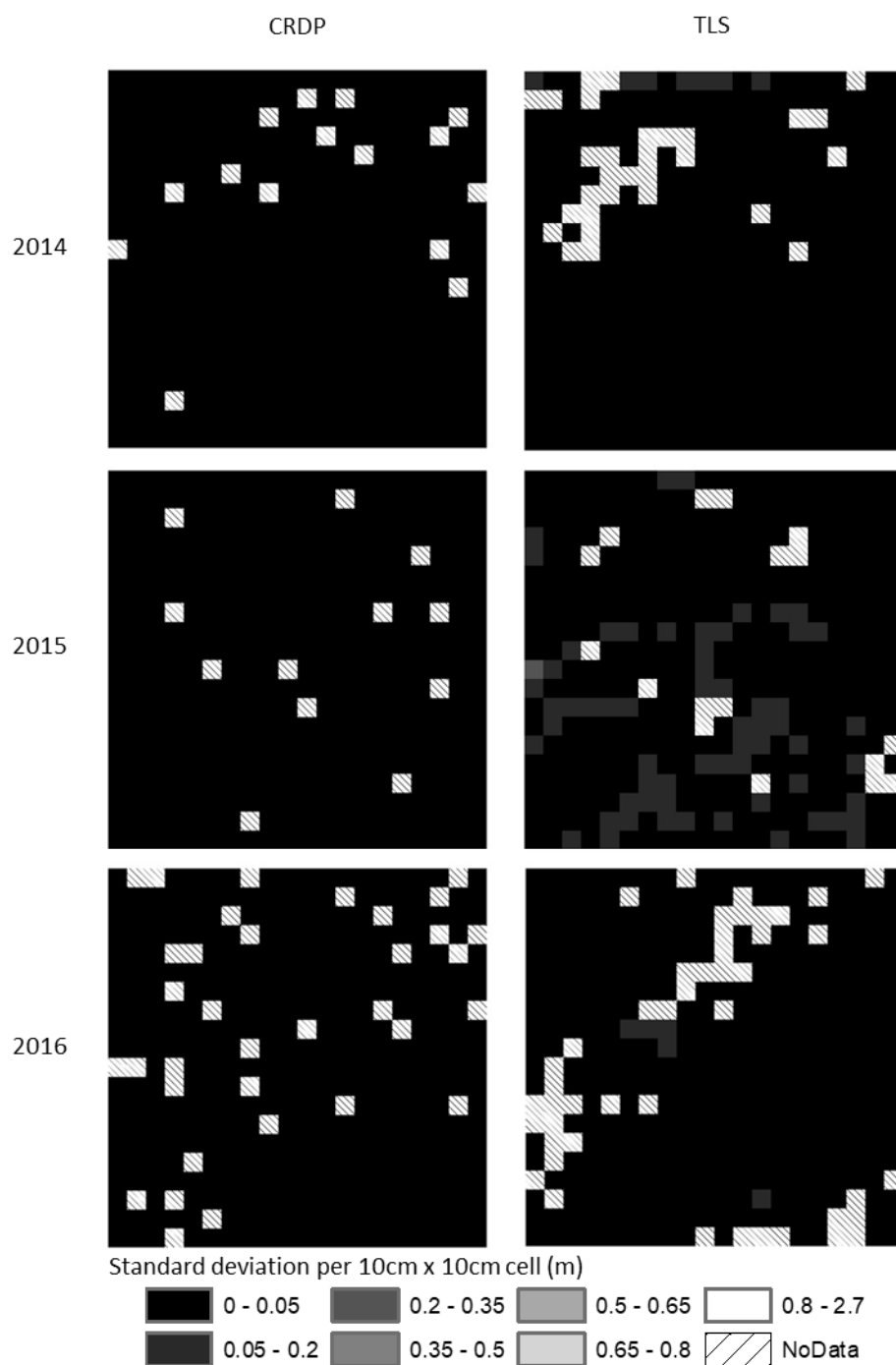   areas are 2 meters long per side

Figure 25   Comparing standard deviation of points between CRDP and TLS 10cm DEM's in typographic area 3 (ground cover and grasses). Small study areas are 2 meters long per side.